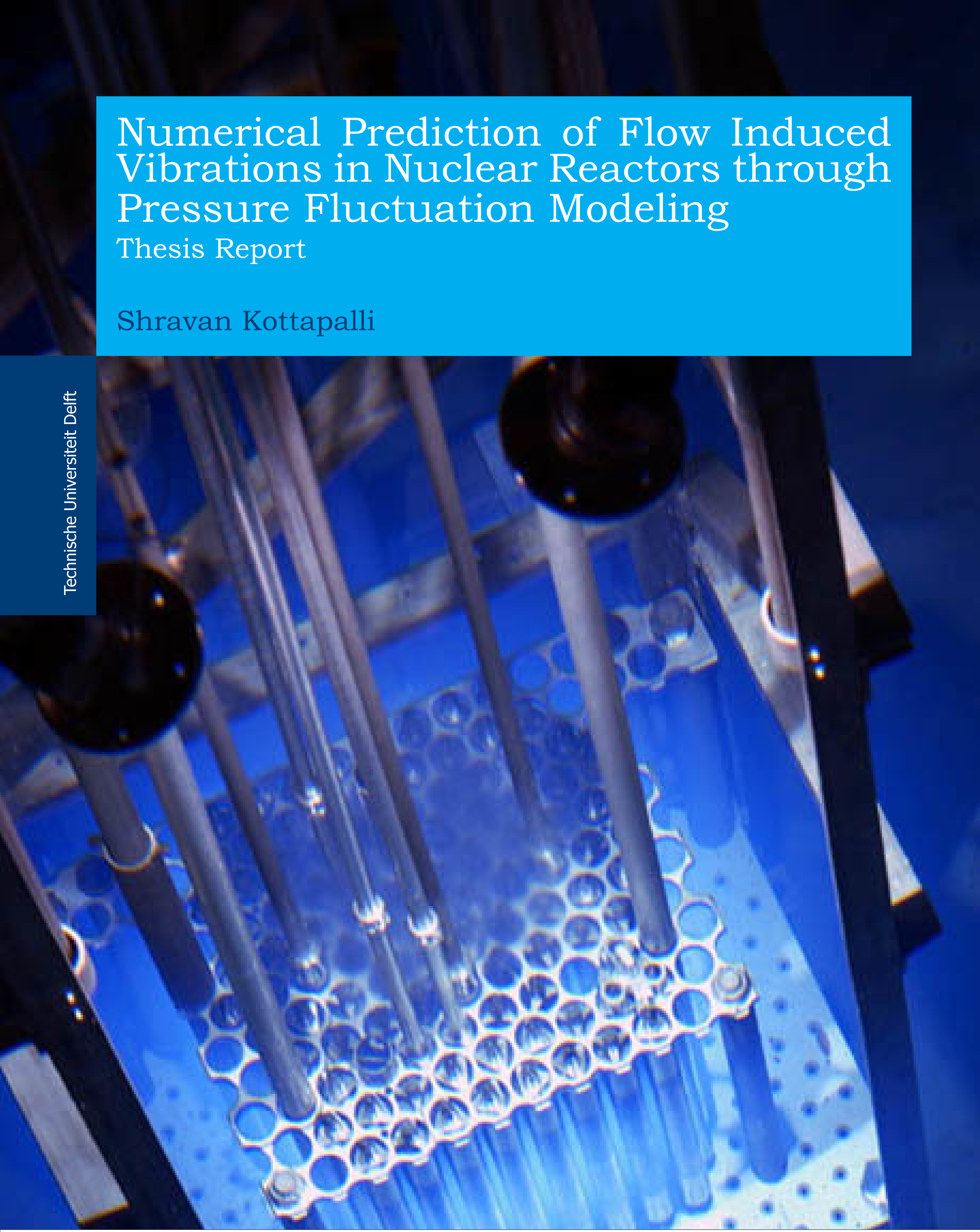

Numerical Prediction of Flow Induced Vibrations in Nuclear Reactors through Pressure Fluctuation Modeling

Thesis Report

Shravan Kottapalli

Technische Universiteit Delft

Delft University of Technology

Challenge the future

Numerical Prediction of Flow Induced Vibrations in Nuclear Reactors through Pressure Fluctuation Modeling

Thesis Report

P&E Report Number: **2798**

by

Shravan Kottapalli

in partial fulfillment of the requirements for the degree of

Master of Science
in Mechanical Engineering

at the Delft University of Technology
to be defended publicly on Tuesday November 29, 2016 at 10:00 AM.

Supervisors:	dr. ir. A. Shams	Nuclear Research and Consultancy Group
	Prof. dr. ir. M. Pourquié	Solid and Fluid Mechanics, 3mE faculty, TU Delft
	Prof. dr. ir. A.H. van Zuijlen	Aerodynamics, LR faculty, TU Delft

Delft
University of
Technology

Acknowledgements

This report is a compilation of the work done for the final year Graduation thesis project. I would like to give a vote of thanks to all the people who have supported me during the course of this work. First, I would like to thank Nuclear Research and Consultancy Group for providing me their support and letting me use their facilities during the course of the project. I would like to sincerely thank my project supervisor at NRG, dr. ir. Afaque Shams for his immense support and motivation. I would like to thank Eline ter Hofstede and Daivd S Blom for taking their time out to help me, whenever I was in need. I would like to thank my Prof. dr. ir. A.H. van Zuijlen and Prof. dr. ir. M. Pourquié from TU Delft to have agreed to supervise me during the course of my Graduation project an providing me with valuable suggestions. I would like to thank the Vattenfall group, Sweden for sharing their experimental results with us and supporting us with the required data. Finally, I would like to thank my family and friends to keep me motivated and provide emotional support during the project.

Shravan Kottapalli
Delft, November 2016

Abstract

Flow induced vibrations (FIV) is a known problem in nuclear reactors. The interaction between the turbulent flow of the coolants and the fuel rod bundles generates vibrations which are undesirable. These vibrations can be a major cause of fatigue failures, stress corrosion cracking and fretting wear of materials, which lead to stand-still costs. Analytical models for FIV are not feasible for complex geometries. This is especially true, when a strong interaction between fluid and structure forces is involved. The dynamic nature and a strong coupling between the two phase generates a need to study FIV by the use of numerical approaches. To take into account the interaction between the fluid and the structure one has to couple the solvers for both the phases. Coupling is achieved by mapping the forces and displacements between the interfaces of fluid and structure domains; also known as the Partitioned coupling. Recent works have made it possible to reduce the coupling errors and make them more efficient through the use of better algorithms.

Due to the wide range of the scales involved, vibrations due to turbulent fluctuations of the flow are particularly challenging to solve. A common approach to this problem is to use high fidelity solvers for fluids such as DNS or LES which are computationally expensive for long and complex domains. Attempts have been made for use of cheaper URANS models to capture the modes of the resulting structural vibration by providing an initial perturbation to the structure. However, URANS models compute the time averaged velocity and pressures. The models do not calculate the effect of pressure fluctuations due to turbulent flow fluctuations on the structure. As a result, URANS does not provide information on the amplitudes of the vibrations of the structure due to turbulent fluctuations.

In the current study, the primary objective is to reduce computational costs, and to still capture the complete dynamic behavior of the structure through the use of URANS models. This is performed by the modeling of pressure fluctuations from the turbulent kinetic energy calculated from the URANS models. The modelled pressure fluctuations (p') are added to the mean pressure ($\overline{p}$), which are then mapped over to the fluid structure interface to generate these vibrations. The method is applied to several test cases related to the field of nuclear energy production and results compared to DNS results and experimental results. The results obtained show that the method is capable of simulating FIV caused due to random pressure fluctuations in a turbulent flow. Form the test cases it was concluded that the method has an advantage of lower cost than LES/DNS, but still has the potential of modelling the amplitude of vibrations by turbulent pressure fluctuations.

Contents

1

Introduction

Nuclear energy has one of the highest energy density per unit mass and volume when compared to all the available sources of energy. This means, that the capacity extractable or usable energy per unit mass or volume of nuclear fuel is the highest. The high energy density of nuclear power makes it a very lucrative and clean way of generating electricity. Significant progress has been made in the field of nuclear science and its application in power generation. However, the risks of handling these potentially hazardous chemicals also should be properly dealt with. The incident at Chernobyl is a constant reminder about the need for nuclear safety. With ever growing demand for power, and the steadily increasing average temperatures on earth; the burden on the fossil fuels has to be reduced. Considering the still developing technologies for complete sustainable solutions, to meet our immediate power demands nuclear power will play an important role in the near future. This also brings the question regarding Nuclear safety. To ensure the safety of nuclear reactors, it is required that all the aspects are under control, and the behaviour of every system is properly studied for all possible conditions. One such reactor component is the fuel rod assembly. In the past, there have been cases of failures in nuclear reactors caused due to the vibrations induced during flow of coolant or moderators. Although extensively studied, it is difficult to predict the flow of a fluid within a reactor. The effect of this flow on the multiple fuel rods that are stacked in a bundle is also unknown.

In the current era of rapidly developing nuclear technologies, the emphasis is also on improving nuclear safety by developing methods which can help industries to better predict the vibrations generated in a system due to fluid flow. The vibrations resulting due to interaction of flow with structural components are known as flow induced vibrations (FIV). Nuclear reactor cores are composed of slender fuel rods that are constantly cooled by flow of coolants around them (refer figure 1.1). The fuel rod assemblies consist of tightly packed group of fuel rods, with pitch (distance between the rod centres) to diameter ratios (P/D) as low as 1. The flow of coolants across such tightly packed rods are usually turbulent in nature, and the turbulence increases with increasing flow rates. These flows under the right conditions can lead to the pressure fluctuations which cause vibration of the rods.

In reactors such as the Sodium cooled, or the Lead cooled fast reactors, the coolant flows across the fuel rods or cylindrical pipes are of higher density compared to Light or Heavy Water. When the density of coolants are small compared to the fuel rods, the effect of these pressure fluctuations are minimal, similarly higher densities of coolants can lead to high displacements of fuel rods. The main phenomenon behind this called the *Added Mass Effect*. This phenomenon leads to a strong interaction between the fluid and the solid or structural components, which have to be taken into consideration during reactor designing. This problem can be potentially dangerous, causing unforeseen damage to the reactors, like fretting wear and damage due to fatigue. The dynamic behaviour prediction of structural components due to external fluid flow becomes more important in Fast reactors, since damages can be more severe.

The first step to understand the problem of FIV is to study the initiation of vibrations due to fluid flow across structural components. Vibrations of any nature in a structure are induced because of an external excitation. Turbulent flow across the structures are the source of random pressure and velocity signals, which provide this excitation. The pressure fluctuations due to turbulent flow externally induced vibrations on the structures, which are known as *Turbulent Induced Vibrations* (TIV). Pressure fluctuations can be either near field or far field, which also depends on the geometry of the flow domain.

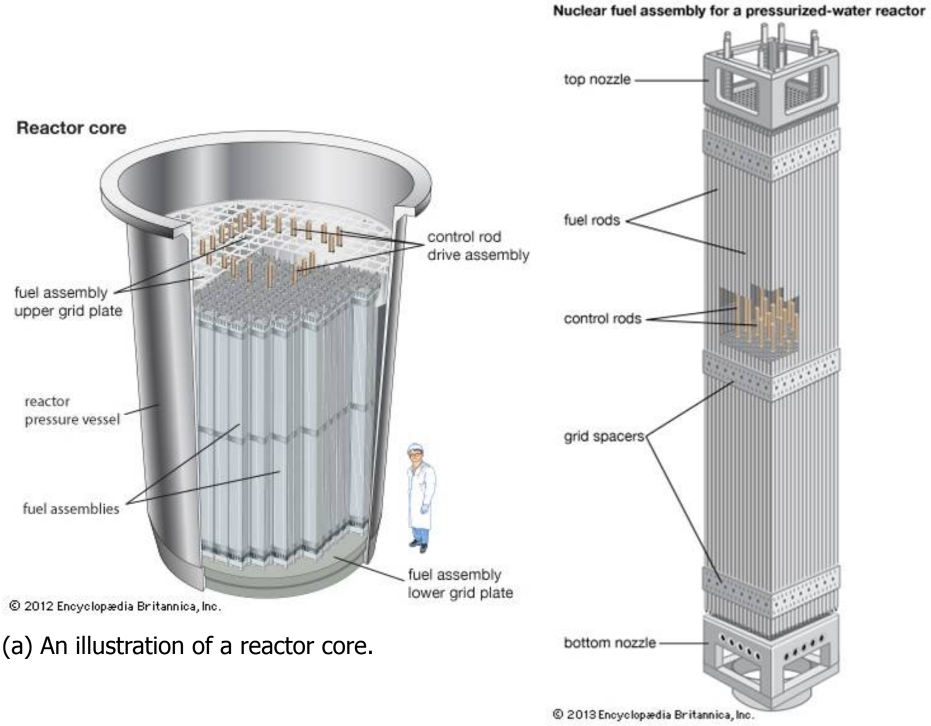

(a) An illustration of a reactor core.

(b) An illustration of a fuel rod assembly.

Figure 1.1: The figures show the components of a nuclear reactor as an example for a fluid-structure problem. The reactor core houses fuel rod assemblies, through which a coolant fluid circulates. It can be observed that the fuel rods in each of these assemblies are placed very close to each other.

The effects of the near and far field pressure fluctuations cause TIV in the case of axial flows, around densely packed rod bundles. To understand these random fluctuations, it is necessary to understand the basics of turbulence and how the effects can be estimated.

1.1. Research Question

The study of TIV is crucial to understand the development of vibrations in a nuclear reactor. Hence, it is of importance to develop tools which can accurately predict TIV. State of the art simulations for TIV are mainly performed using high fidelity CFD (Computational Fluid Dynamics) solvers such as DNS (Direct Numerical Simulations) or LES (Large Eddy Simulations). These CFD (Computational Fluid Dynamics) codes are coupled to a suitable CSM (Computational Solid Mechanics) solver for simulating vibrations on structures due to fluid flow. However, these simulations can be expensive due to high demands of memory and computational power. This brings the main objective of the study into perspective.
Is it possible to simulate Turbulence Induced Vibrations using low fidelity solvers such as Unsteady-RANS models?

To find the answer to the question a literature review was performed to study upon all the aspects of Flow induced vibrations, Fluid Structure interaction and Turbulence Modeling. The study also involves exploring other methods which have been developed to simulate TIV. All the aspects of the literature review have been compiled in chapter 2 to chapter 4. Later, a new approach to simulate TIV will be discussed in chapter 5. Finally, after answering the above mentioned questions, the results of the study are put forth and the conclusions from the same are drawn in chapter 6 and chapter 7.

2

Flow Induced Vibrations

Safety of Nuclear reactors is of paramount importance to prevent environmental and financial damage. In nuclear power plants, flow induced vibration (FIV) may cause safety issues such as fatigue problems, stress corrosion cracking, possible failure modes and fretting wear. This may eventually leads to nuclear safety issues and substantial standstill costs due to unplanned outage. The focus of this report is on the damage caused due to the internal forces exerted by the fluid flow on the structural components within a nuclear reactor. In the past there have been recorded cases of damage or shutdowns in reactors due to vibrations caused in the structural components. The origin of these vibrations is due to the interaction between the flow of the fluid (moderator or coolant) and the reactor components. This phenomenon is commonly termed as Flow Induced Vibrations (FIV). In this current chapter, more light will be shed on the details of research being carried out in this field and on the ways of predicting this phenomenon.

2.1. History of FIV research

FIV has been a topic of research in many fields. Many practical problems related to FIV have been observed in industrial fields such as mechanical systems, civil engineering, aeroplanes, ships and nuclear power plants. The drag direction vibration of a thermocouple well in the Fast Breeder Reactor at *Monju* in Japan, is one such example. This was caused due to systematic vortex shedding as stated in the book by the Japanese Society of Mechanical Engineers (JSME) [1]. Two main conferences related to FIV were held in 1972 and 1979 by the initiative of Prof. Naudascher of University of Karlsruhe, Germany. FIV phenomena can be classified into two main types: steady flow induced and unsteady flow induced. Since the year 1990, *The Yayoi research seminar* in University of Tokyo, Japan has been held every year to present the current developments in FIV research related to nuclear reactor applications. Major meetings related to FIV are also conducted by the American Society of Mechanical Engineers (ASME) the *International Symposium on Fluid-Structure Interactions, Aeroelasticity and Flow-Induced Vibration & Noise* every 4 years. In Europe, the *International Conference of Flow-Induced Vibrations* is also conducted in every 4 years.

2.2. Types of induced vibrations

Flow induced vibrations or FIV can cause accelerated degradation or damage to structural components reacting with the flow of the fluid involved. Most component structural designs do not consider the dynamic forces of the fluid flow on structural components. This can lead to early problems in reactors and also lead to major safety concerns. After decades of work, there has been significant development in ways of predicting the effects of FIV by usage of vibration models. Predicting dynamic behaviour of structures by wrong vibration models can lead to an un-optimal design. FIV can lead to fretting wear and fatigue failures in components even before their estimated design life, causing maintenance issues and frequent shut downs. FIV can be roughly divided into five fields [1] -

- Vibration induced by Cross-flow.

- Vibration induced by parallel flow or external axial flow.
- Vibration of piping conveying fluid, due to pressure fluctuation, and thermal excitation.
- Fluid-Structure Interaction.
- Vibration of Rotating structures in flow.

Vibrations caused in the nuclear reactor rod bundles and other heat exchanger applications are mainly due to crossflow and parallel flow induced vibrations. Due to the higher efficiency of parallel flow type heat exchangers, majority of Nuclear reactors are of parallel flow type. Therefore, vibrations due to parallel flow would be dealt with more in detail.

2.3. Classifications and mechanisms of vibrational response

To predict the vibrations due to FIV, the modelling approach used is very important. A wrong modelling approach would quite possibly lead to wrong results, and ultimately to a faulty design. Figure 2.1 shows some of the basic modelling approaches for FIV. Depending on the problem, the modelling of the fluid flow across the solid body can be used to predict the flow and the dynamic forces acting on the structure can be calculated.

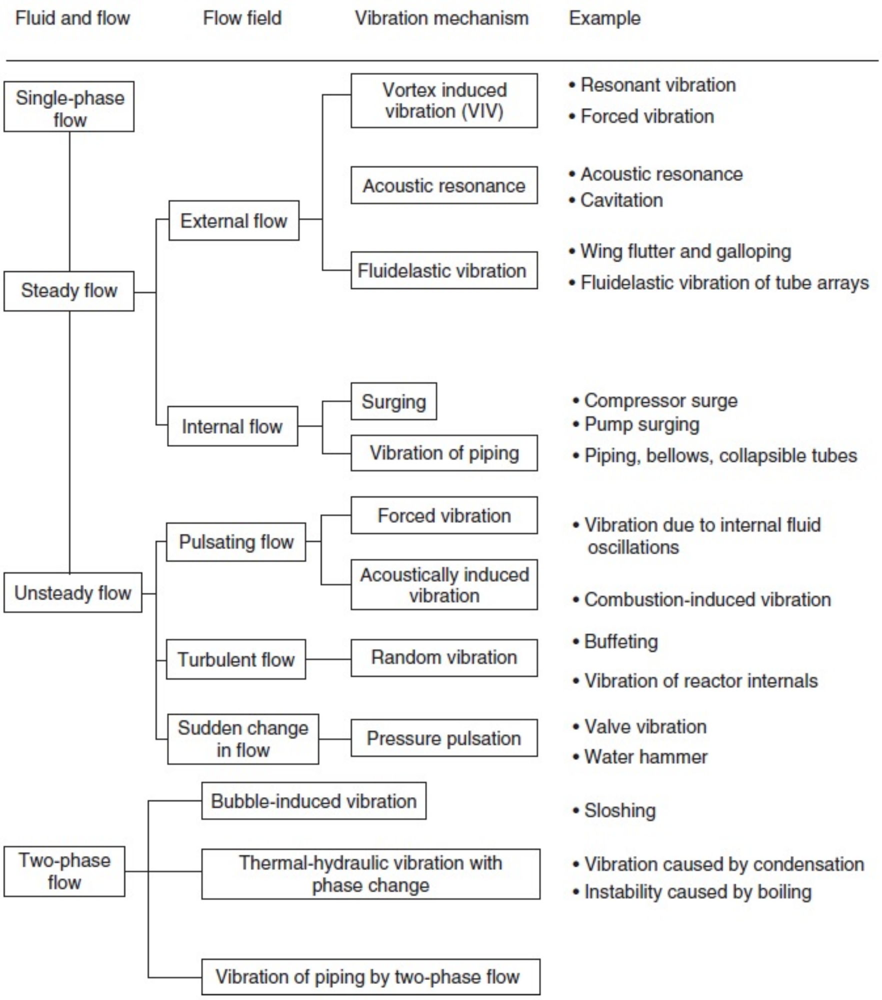

Figure 2.1: Classification of FIV mechanisms [1].

By coupling characteristics of a fluid flow to the material behaviour of the solid, it is then possible to simulate FIV. The response of the structural components is modeled for different conditions; like Vortex Induced vibration, Fluid-elastic instability and vibrations due to random pressure fluctuations. After the response is modelled for each type, the responses can then be super imposed to predict the final behaviour of the structure in relation to the flow. This has been explained by the figures 2.2a and 2.2b.

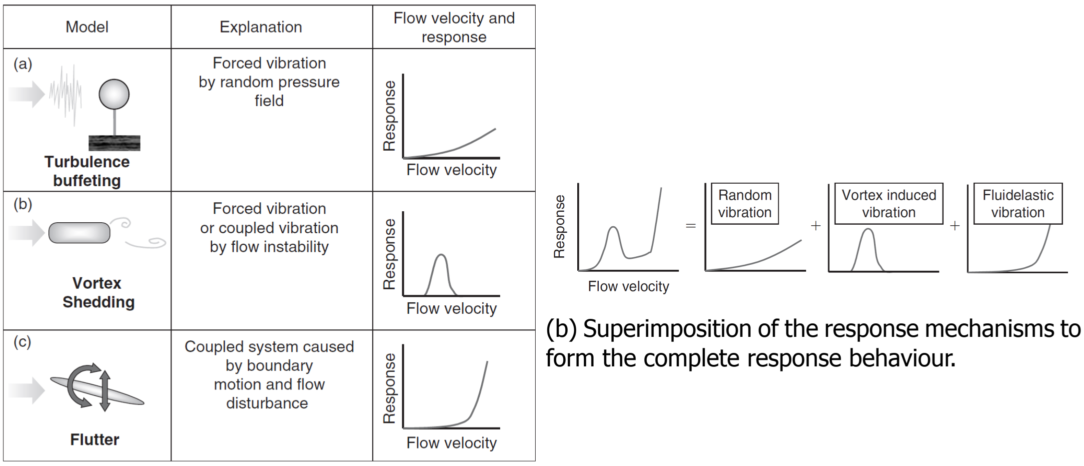

(a) Various fluid-structure mechanisms for external flows.

(b) Superimposition of the response mechanisms to form the complete response behaviour.

Figure 2.2: An example on determining the response behaviour of structure due to external flow of a fluid [1].

The case depicted above shows that for a typical cross flow induced vibrations, there are three major types of vibration models. In a parallel flow conditions, vibrations due to vortex shedding are usually absent. Flow induced vibrations are mainly initiated due to the random pressure fluctuations generated due to turbulent flow. Once the vibrations are induced, higher turbulence can then lead towards an acoustic resonance of the structure with mean pressure of the flow and can even further develop towards fluid elastic instability.

2.4. Vibrations induced by parallel flow

When nuclear fuel bundles and steam generators are subjected to parallel flow, instabilities such as flutter can happen at high flow velocities. In parallel flow conditions, the critical flow velocities required for fluid elastic instabilities to occur, are higher than for cross flow conditions. This means, vibrations due to fluid flow are lower for parallel flow, when compared to cross flow for the same mass flow rate of fluid. In a parallel flow, vibrations are caused due to two main types of phenomenon.

The first type of vibrations are caused due to random pressure fluctuations, which are caused due to turbulent flow around the structure. Initiation of turbulence is mainly caused due to geometry of the duct and/or due to the wall friction of the duct. Introduction of turbulence within in the flow is the main origin of pressure fluctuations at fluid structure interface. Since the vibration on the structure is forced due to external pressure fluctuations, it is generally known as *Externally Induced Excitation* (EIE). When, EIEs are generated due to turbulence, they are known as *Turbulence induced vibrations*, which will be covered in more detail in Chapter 4.

As the velocities of fluid across the structures keeps on increasing, the inertial and viscous forces of fluid begins to dominate over the random pressure forces, and the effect of turbulence on the vibrations is then reduced. The velocity threshold at which the these forces are start to dominate depends on the the material properties of the fluids and structures, and also on the internal forces of the structures (due to stiffness of the structure). This velocity threshold is also known as the *critical velocity*. The instabilities caused due to the interaction between these inertial and viscous forces of the fluids and the structures, are known as *Fluid Elastic Instabilities*. A simplified explanation of this phenomenon can be found in section 2.5. Since, these instabilities are dependent on the interaction between the fluid and structural forces, the interaction also decides the strength of coupling between the two phases.

2.5. Fluid Elastic Instabilities

Fluid Elastic Instabilities are generated when dynamic forces from the fluid flow and the dynamic forces from the structure start interacting with each other leading to self excited vibrations. In many cases fluid elastic instabilities amplifies the vibrations as the flow velocity increases. The phenomenon that couples these interacting forces are the *Added Mass Effect* and the *Stiffness ratio* between the solid and the fluid materials. The concept of Added Mass is explained in more detail by the following example of piston-cylinder system.

Added Mass Effect

Figure 2.3 depicts the domain and the terminology used in the equations mentioned below. The piston is connected to a spring-damper system. The mass of the spring-damper system is assumed to be negligible compared to the mass of the piston. The cylinder consists of a fluid which is then pushed by the spring-mass system out of the outlet Γ_o. The dimensions and other characteristics of the domain have been shown in the mentioned figure.

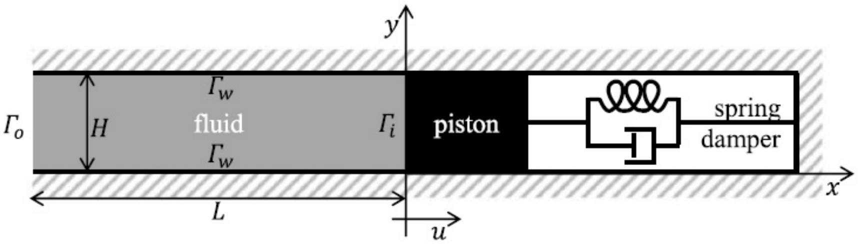

Figure 2.3: The domain for the piston-cylinder system [2]. The u shown in the figure refers to the displacement of the piston. The boundaries of the fluid domain are given by Γ_i, Γ_o and Γ_w for the inlet, outlet and the walls of the fluid domain (Ω_f) respectively.

For an inviscid and incompressible fluid, equations 2.1 and 2.2 define the one dimensional momentum and continuity equations

$$\frac{\partial v}{\partial x} = 0 \tag{2.1}$$

$$\rho_f \frac{\partial v}{\partial t} + \rho_f \frac{\partial v v}{\partial x} = -\frac{\partial p}{\partial x} \tag{2.2}$$

in Ω_f. The boundary conditions for the flow at outlet Γ_o and the fluid-structure interface Γ_i are

$$p = f(t) \text{ on } \Gamma_o \tag{2.3}$$

$$v = \frac{\mathrm{d}u}{\mathrm{d}t} \text{ on } \Gamma_i \tag{2.4}$$

The boundary condition on the wall Γ_w is not taken into consideration since this is a one dimensional problem. The equation of the structure is given by

$$m\frac{\mathrm{d}^2 u}{\mathrm{d}t^2} + c\frac{\mathrm{d}u}{\mathrm{d}t} + bu = Hp_i \tag{2.5}$$

The mass of the piston is indicated by m, the damping constant is denoted as c and the spring stiffness factor is b. Then the pressure on the fluid-structure interface Γ_i is given by p_i.

The fluid velocity is eliminated from the equations 2.1 and 2.2, giving

$$\frac{\partial^2 p}{\partial x^2} = 0 \text{ in } \Omega_f \tag{2.6}$$

$$p = f(t) \text{ on } \Gamma_o \tag{2.7}$$

$$\frac{\partial p}{\partial x} = -\rho_f \frac{\mathrm{d}^2 u}{\mathrm{d}t^2} \text{ on } \Gamma_i \tag{2.8}$$

The boundary conditions on Γ_i is obtained by substituting equations 2.3 and 2.4. The solution of the equations 2.6 and 2.7 and 2.8 is given by

$$p(x,t) = f(t) - \rho_f (L + x) \frac{\mathrm{d}^2 u}{\mathrm{d}t^2} \tag{2.9}$$

Substituting in Eq. 2.5 results in

$$m \frac{\mathrm{d}^2 u}{\mathrm{d}t^2} + c \frac{\mathrm{d}u}{\mathrm{d}t} + bu = H(f(t) - \rho_f L \frac{\mathrm{d}^2 u}{\mathrm{d}t^2}) \tag{2.10}$$

which can be rewritten as

$$(m + m_a) \frac{\mathrm{d}^2 u}{\mathrm{d}t^2} + c \frac{\mathrm{d}u}{\mathrm{d}t} + bu = Hf(t) \tag{2.11}$$

where the term, $m_a = \rho_f HL$ is the *Added-Mass* or the virtual mass.

The virtual or *Added mass* leads to a higher deceleration of the piston during its acceleration and deceleration. Due to this a higher resisting force is applied in the equal and opposite directions, changing the overall natural frequency of the system. The natural frequency at which the spring vibrates changes according to the density of the fluid displaced by the piston. Degroote [2] in his paper formulates the expression for the natural frequency of the spring mass system.

The natural frequency of the piston cylinder system, changes from ω to $\tilde{\omega}$ due to the added mass $m_a = \rho_f HL$

$$\omega = \sqrt{\frac{b}{m}} \text{ and } \tilde{\omega} = \sqrt{\frac{b}{m + m_a}} \tag{2.12}$$

The change in the natural frequency here can hence be clearly observed. The density of the surrounding fluid is a very important factor on the interacting forces between the solid and fluid. To measure the effect of added mass on the dynamic behaviour of a solid the *Density Ratio*

$$\text{Density Ratio} = \frac{\rho_{solid}}{\rho_{fluid}}$$

is a non dimensional number that gives a good estimation of the coupling strength. The lower the value of Density Ratio, the higher is the dynamic interaction or *stronger the coupling* between the forces of the solid and fluid. Density Ratio is one of the parameters defining the strength of coupling between interacting forces.

Effect of Stiffness on the coupling

In the case of structures like beams, the strength of coupling also depends on the stiffness of the beam. Stiffness of a structure is a function of the material properties of the structure and the geometry of the structure. In an article by Liu et al. [3], FIV was simulated with various rod configurations. The simulations was carried out with three main non-dimensional parameters.

$$Re = \frac{\rho v_o D_h}{\mu} \tag{2.13}$$

$$\overline{U} = v_o L \sqrt{\frac{\rho A_t}{EI}} \tag{2.14}$$

$$\beta = \frac{\rho A_t}{\rho A_t + \rho A_e} \tag{2.15}$$

where Re, $\overline{U}$, and β are the Reynolds number, dimensionless flow velocity and mass ratio respectively. v_o and D_h are the average flow velocity and hydraulic diameter; L, A_e and A_t are the length, effective cross sectional area of each beam (rod) and the total cross sectional area.

Here the effect of the stiffness on the flow has been used in the non-dimensional flow velocity parameter $\overline{U}$. This parameter has been obtained from the dynamic equation of the beam considering Euler-Bernoulli beam theory [4]. A lower stiffness means a more flexible structure which deforms readily when subjected to external fluid forces. Such problems are strongly coupled and hence require a robust and stable coupling algorithms.

3

Fluid and Structure Coupling

Flow induced vibration is an unsteady phenomenon. Flow exerts pressure forces on the structural components, which respond by exerting an equal and opposite force. The response of the structure is then dependent on the fluid properties and the flow behaviour. These forces are in a constant interaction which leads to vibrations on a structure. In section 2.5, it was seen on how the structural response of a solid is dependent on the interacting fluid. Dynamic behaviour of some structural components due to the fluid can be calculated analytically by making assumptions such as, negligible viscosity, a steady state flow or the fluid being incompressible. However, these assumptions do not hold when the forces acting on the fluid and structures are strongly inter-dependent. To deal with such complexities, simulating the problems by numerically solving the governing equations is a novel approach. Numerical methods used in such cases require coupling of Computational Fluid Dynamics (CFD) solvers to solid CSM solvers (Computational Solid Mechanics solvers) to calculate the effects of the dynamic forces of the fluid on the solid.

FIV in nuclear reactors, involve strong coupling between fluids and structures. The density ratios in these cases can vary from as high as ≈ 8 (steel - water) to ≤ 1 (steel - Lead Bismuth Eutectic). These lead to strong coupling cases and hence need a robust and efficient coupling method. In this chapter we will explore all the various coupling schemes that are put to use to solve such problems and then choose one of the coupling schemes suitable for the application.

3.1. Methods for solving Fluid Structure problems

To solve a fluid structure problem numerically, a monolithic or a partitioned approach can be used. Monolithic solvers solve the fluid and the structure equations simultaneously. This makes them ideal to solve fully coupled problems of fluid and structure problems. These solvers do not need to couple different solvers and hence avoid the errors due to the numerical schemes implemented for coupling the fluid and solid solvers independently. However, monolithic solvers are problem specific, they cannot be directly used for different types of problems and lose greatly on modularity of the solvers. Therefore, monolithic solvers are not economical to solve problems with weak or moderately strong coupling.

The second type of coupling method is the partitioned coupling method. These solvers employ the use of coupling algorithms to couple two black-box solvers. Partitioned coupling algorithms perform active data exchange and mapping the solvers, through one-way or two-way data exchange and constantly adapt the solution to changing boundary conditions. Such methods involve introduction of a coupling error in the simulation which depends on the numerical scheme employed. Since the coupling schemes act as an add-on to a pre-existing set of solvers, it is a more flexible approach for the current application. There are several coupling algorithms that have been developed in the past years and a few of them have been discussed in this chapter.

To give an idea of how the methods work, we can consider an example of a coupled system involving a piston-cylinder problem, where the piston (the mass) is attached to a spring (refer figure 3.1). The piston is connected to spring-mass system, with the piston as the main mass. When a small displacement is provided to the piston, it compresses the gas inside pressuring the cylinder. To balance the

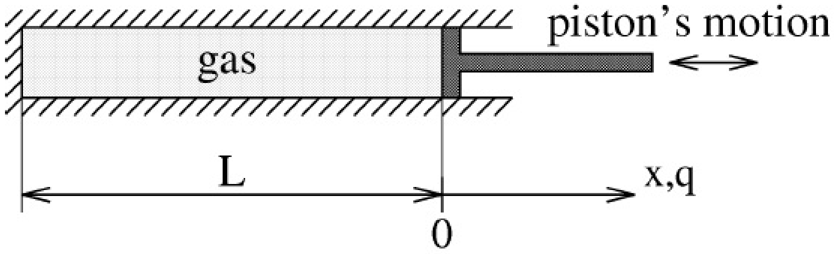

Figure 3.1: Domain of a piston and cylinder problem [5]. The piston (main mass) is connected to a spring, and the cylinder contains a fluid that is compressed due to inward motion of the piston.

force, the pressurised cylinder exerts a counterforce on the piston. This creates a fluid-solid interaction between them. Figure 3.2a, explains the workflow of monolithic coupling. It can be observed that monolithic coupling solver solves all the system equations simultaneously. Partitioned solvers employ different solvers to solve the problems separately, and rely on a coupling algorithm to exchange and map data between the solvers at the interface. The coupling is done both in space and time, which can be seen in figure 3.2b.

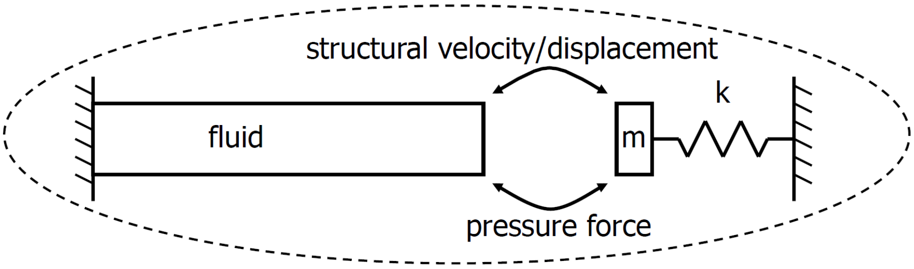

(a) Monolithic approach of solving an FSI problem.

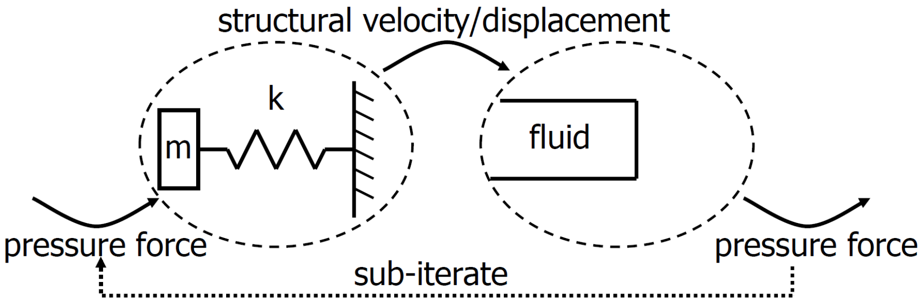

(b) Partitioned approach to solving an FSI problem.

Figure 3.2: Approaches to solving FSI problems [5].

Due to the flexibility and ease of use, partitioned solvers are more popular compared to monolithic solvers, and are widely used in commercial packages. New methods for coupling black-box solvers are currently being studied to produce accurate and stable methods for fully coupled problems.

3.2. Coupling algorithms

Partitioned coupling algorithms have been widely used in many solvers. Most of the CFD solvers have a segregated and a coupled methods of solving a flow problem. Segregated methods solve velocity and pressure terms separately and iterate for convergence, whereas coupled solvers solve for the complete Navier-Stokes equation. A similar analogy can be applied to couple fluid and solid solvers. Temporal coupling or *Coupling in time* forms the basis of this discussion. Partitioned coupling algorithms are mostly classified into two types based on the coupling, namely *Basic or Weak Coupling schemes* or also known as the *One-way Coupling*; and the *Sub-Iterated or Strong Coupling schemes* also known as the *Two-way Coupling*.

3.2.1. Basic coupling

For weakly coupled problems, the interaction is dominated by either the structure or the fluid medium. For instance, in the case of an aluminium cantilever beam vibrating in air, the natural frequency of the beam is hardly affected due to the flow of air around the beam. This is due to its weak pressure forces, or low added mass effects. This can be classified as an example of a weakly coupled Fluid-structure problem.

To solve such cases, the coupling can be performed by one direction (or one-way) data exchange between the solvers (solid to fluid), rather than both directions. This sort of coupling is known as *Basic or Weak coupling*. The coupling scheme calculates of the values of the next time step directly based on the values of the previous time step without any iterations. Therefore, sometimes these schemes are also known as *Explicit Coupling*.

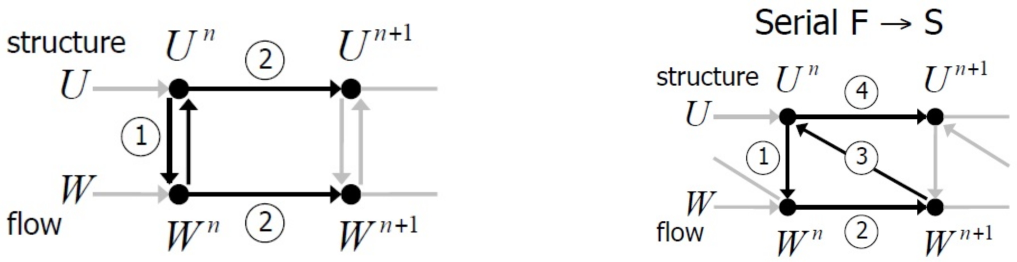

(a) Explicit Parallel coupling scheme (Jacobi).

(b) Explicit Serial scheme (Gauss-Seidel).

Figure 3.3: fig: Basic partitioned Coupling schemes [5] for weakly coupled problems. Note that the data exchange between both the coupling method is performed only once every time-step.

In explicit coupling, the data exchange is done only once with each time step and is performed only in one way. Basic coupling is easy to implement and is an efficient coupling method due to lower calculation time. Two main types of explicit coupling schemes are parallel and serial coupling schemes. When the interaction between the fluid and solid is strong, explicit schemes are unstable and require smaller time steps to keep the coupling stable. Therefore, to solve strong coupling problems, explicit coupling are seldom used.

3.2.2. Sub-Iterated coupling

Sub-iterating schemes are put to use when there is a strong dynamic coupling between the fluid and solid. As the name suggests, these schemes use sub-iterations within each time step. The data is mapped and exchanged between the solvers multiple times within a time step to achieve convergence. Figure 3.4 shows the exchange of data during every iteration. Due to the multiple sub-iterations within one time step, the scheme is also known as *Implicit Coupling*.

(a) Sub-iterated Parallel coupling scheme.

(b) Sub-iterated (Structure to Fluid) Serial coupling scheme.

Figure 3.4: fig: Sub-Iterate Coupling schemes [5]. The dotted lines in the diagrams depict multiple data exchanges within each time-step to converge to a solution. The parallel and serial coupling schemes have been explained in detail in

Sub-iterating in each time-step increases the computational time required for the solution to converge per time-step. However implicit coupling methods is more stable than explicit coupling. This allows for larger time-steps than explicit coupling. This makes implicit methods more efficient when dealing with strong coupling cases.

Implicit coupling schemes can be further subdivided based on their coupling algorithms. Two of the commonly used coupling algorithms are

- Parallel Coupling (Jacobi Scheme)
- Serial Coupling (Gauss-Seidel Scheme)

These coupling schemes are covered more in detail in the following sections. Apart from the mentioned schemes, some new iterative methods will also be discussed which are proven to be efficient for solving strongly coupled problems, namely the *Quasi-Newton and Block-Quasi Newton Methods*.

3.3. Jacobi iteration

The Jacobi iteration scheme is a popular scheme to solve a set of equations iteratively. The scheme involves a guess to initialize all the variables, followed by the calculation of residuals. Using these residuals of the previous iteration, the values for the next iteration is calculated. The iterative process continues till the value of residuals fall below the required tolerance (refer to figures 3.3a and 3.4a). The complete method in equation 3.1. U and W are the structural and fluid domain variables respectively. A_s and A_f are the matrices for solving the fluid and solid equations, while A_{sf} and A_{fs} are the coupling matrices between fluid to structure and structure to fluid respectively.

$$\text{Jacobi (parallel) scheme: } \left[I - \Delta t \begin{pmatrix} A_s & 0 \\ 0 & A_f \end{pmatrix}\right] \begin{pmatrix} U^{k+1} \\ W^{k+1} \end{pmatrix} = \begin{pmatrix} U^k \\ W^k \end{pmatrix} + \Delta t \begin{pmatrix} 0 & A_{sf} \\ A_{fs} & 0 \end{pmatrix} \begin{pmatrix} U^k \\ W^k \end{pmatrix} \tag{3.1}$$

where the superscript k signifies the k^{th} iteration in solving the equations. As, values of U and W for the next iteration are updated after solving the complete set of equations, this method is also known as the *Parallel Iteration Scheme*. Mathematically this scheme is represented in the following manner, consider a set of equations,

$$Ax - b = 0 \tag{3.2}$$

then, for k^{th} iteration Jacobi equation can be written as,

$$x_i^k = \frac{1}{a_{ii}} \left[\sum_{j=1}^{n} \left(a_{ij} x_j^{k-1} \right) + b_i \right] \tag{3.3}$$

which in matrix form would be,

$$x^k = D^{-1}(L + U)x^{k-1} + D^{-1}b \tag{3.4}$$

where, $A = D - L - U$, D is the diagonal matrix, L is the lower triangular matrix and U is the upper triangular matrix. Therefore, the coupling equations for the solid and fluid solvers by Jacobi method are represented as,

$$W^{k+1} = F(U^k) \tag{3.5}$$

$$U^{k+1} = S(W^k) \tag{3.6}$$

where, W^k are the fluid properties at k^{th} iteration and U^k are the solid properties at k^{th} iteration. $S(W^k)$ and $F(U^k)$ represents the functions for the structural solver and the fluid solver respectively. The structure solver is a function of the flow properties (W) and the fluid solver is a function of the structural properties (U).

3.4. Gauss-Seidel

The Gauss-Seidel iteration scheme is a popular iteration scheme to solve a system of equations. In this scheme, the initial value of the variables are estimated for the first equation and updated in the successive equation. The residuals are calculated after the complete system of equations are updated. The calculated residuals are used to calculate the estimate for the next iteration. Therefore, this type of iteration method is also known as the serial scheme. Generally the Gauss-Seidel method is found to be more efficient than the Jacobi scheme. The whole equation can be written down in the following manner, the terms mentioned below have the same meanings as for equation 3.7.

$$\text{Gauss-Seidel (serial) scheme: } \left[I - \Delta t \begin{pmatrix} A_s & A_{sf} \\ 0 & A_f \end{pmatrix}\right] \begin{pmatrix} U^{k+1} \\ W^{k+1} \end{pmatrix} = \begin{pmatrix} U^k \\ W^k \end{pmatrix} + \Delta t \begin{pmatrix} 0 & 0 \\ A_{fs} & 0 \end{pmatrix} \begin{pmatrix} U^k \\ W^k \end{pmatrix} \tag{3.7}$$

Mathematically this can be shown by considering the same set of equations as shown in equation 3.2. Then for k^{th} iteration the Gauss-Seidel iteration can be shown as,

$$x_i^k = \frac{1}{a_{ii}} \left[\sum_{j=1}^{i-1} \left(a_{ij} x_j^k\right) - \sum_{j=i+1}^{n} \left(a_{ij} x_j^{k-1}\right) + b_i \right] \tag{3.8}$$

in matrix formulation, the equation can be written as,

$$x^k = (D - L)^{-1} U x^{k-1} + (D - L)^{-1} b \tag{3.9}$$

with D, L, U having the same meaning as equation 3.4. Therefore, for coupling of solid and fluid solvers a similar approach is used by solving the fluid equations first and updating the obtained result in the structure equations.

$$W^{k+1} = F\left(U^k\right) \tag{3.10}$$

$$U^{k+1} = S\left(W^{k+1}\right) \tag{3.11}$$

$$\therefore W^{k+1} = SoF\left(W^k\right) \tag{3.12}$$

where k, $F(U^k)$ and $S(W^k)$ are the iteration level, function for the fluid solver and function for the structural solver respectively. The function $SoF(U^k)$ is equivalent to a nested function $S(F(U^k))$. An interesting fact to be observed is that in equation 3.12, the value at the next iteration level of the coupling is a function of itself in the at the previous time step. This property of the coupling scheme is known as the *Fixed Point Iteration* property. Figures 3.3b and 3.4b show how the equations are solved in the basic and sub-iterated types of serial coupling. A general coupling loop of a Gauss-Seidel iteration is given in the following manner [2],

```
while $|r^k| \geq$ tolerance
    $\tilde{x}^k = x^{k-1} + r^k$
    $x^k = SoF(\tilde{x}^k)$
    $r^k = x^k - \tilde{x}^k$
```

where r^k is the residual at the k^{th} iteration.

To make the convergence of the G-S scheme more stable an under-relaxation factor quite often used. The under-relaxation factor reduces large jumps in the values of the next iterations due to large residuals. This greatly reduces fluctuations in the convergence of the residual, although at the expense of decrease in convergence rates. Under-relaxation factors are employed in the equation as follows,

$$\tilde{x}^k = x^{k-1} + \omega r^k \tag{3.13}$$

where,ω is the under-relaxation factor. Instead of using a constant under-relaxation factor an adjustable under-relaxation factor can also be used which can adjust itself according to the convergence rate of the residual.

3.4.1. Aitkens under-relaxation

The Aitkens under-relaxation method is an adaptive method, in which the information from the residuals of consecutive iterations are used to predict the under-relaxation factors for the next iteration. This is a useful method to increase the efficiency of the Gauss-Seidel scheme. This method calculates the steepest descent to the minimise the number of iterations required for the solution to converge and adapts the under-relaxation factor accordingly. The Aitkens under-relaxation scheme is as follows [2],

$$\omega^k = -\omega^{k-1}\frac{\left(r^{k-1}\right)^T\left(r^k - r^{k-1}\right)}{\left(r^k - r^{k-1}\right)^T\left(r^k - r^{k-1}\right)} \tag{3.14}$$

where, ω^k is the under-relaxation factor for the k^{th} iteration, and r^k is the residual for the k^{th} iteration.

3.4.2. Stability of Gauss-Seidel coupling

The Gauss-Seidel method is a first order coupling method, which means, it does not involve the use of derivatives (Jacobian or Hessian). Due to this, the coupling scheme can get unstable even with low under-relaxation factors. Stability of the Gauss-Seidel method depends on the following parameters,

- Time-step:
  The Gauss-Seidel method tends to get unstable with smaller time steps. This causes a problem when fluid or solid solvers require small time-steps for each individual solver to remain stable and reduce errors. One way around this problem is by sub-cycling, which allows for higher coupling time-steps, but this can compromise the accuracy of the solution.
- Under-relaxation factor:
  A lower under-relaxation factor reduces the fluctuations in the residual of the solution leading to a better convergence. Low under-relaxation factors can increase the required number of iterations for the solver to converge, making it less efficient.
- Initial Guess or pre-conditioner:
  A good initial guess for the coupling scheme can greatly improve the efficiency and stability of the coupling method. These can be obtained by calculating the approximate initial guess roughly, which would form the base for the iterations. A bad initial guess could even lead to divergence of the coupling scheme.
- Material properties of solid and fluid:
  For strong coupling simulations involving dense, incompressible fluids, the Gauss-Seidel method can get unstable. One way of making the simulation more stable is by assuming the fluid to be compressible. The compressibility of the fluid can be can be controlled by writing user-defined functions, which would then govern the density of the fluid. This method is can be helpful when dealing with simulations having low density ratios.

3.5. Quasi-Newton Methods

The Gauss-Seidel coupling method and Jacobi method are first order methods to find the *Zero* of the residual function, since there is no involvement of derivatives. Quasi Newton methods are second-order methods. Apart from the values of the residual calculated, these also rely on calculating the derivatives of residual function to attain faster convergence. To explain the significance of this, we consider the following set of equations to solve for a quantity p.

$$\begin{aligned}
&\tilde{p}^k = p^{k-1} + \Delta p^k \\
&p^k = SoF\left(\tilde{p}^k\right) \\
&R\left(p^k\right) = p^k - \tilde{p}^k \\
&\text{For } R(p) = 0, \text{Linearising the residual function gives,} \\
&\left(\frac{\partial R}{\partial p}\right)\Delta p^{k+1} = -R\left(p^k\right) \\
&\therefore \Delta p^{k+1} = -\left(\frac{\partial R}{\partial p}\right)^{-1} R\left(p^k\right)
\end{aligned} \tag{3.15}$$

here, the residual function for the solution of p is given by $R(p)$. To find a $Zero$ of this residual function the Jacobian would be given by $\mathcal{J} = \left(\frac{\partial R}{\partial p}\right)$. The main reason on why Gauss-Seidel method is a first-order method is because it considers the Jacobian to be an identity matrix (I), $\left(\frac{\partial R}{\partial p}\right)^{-1} = -I$. So the k^{th} iteration to solve for p would be given by [5],

$$\tilde{p}^k = p^{k-1} - \Big(-I\Big)R(p), \qquad \text{...Gauss-Seidel method} \tag{3.16}$$

$$\tilde{p}^k = p^{k-1} - \Big(-\omega I\Big)R(p), \qquad \text{...G-S with fixed under-relaxation} \tag{3.17}$$

$$\tilde{p}^k = p^{k-1} - \Big(-\omega^k I\Big)R(p), \qquad \text{...G-S with Aitkens under-relaxation} \tag{3.18}$$

However, if the value of the Jacobian is calculated it leads to faster convergence and the method is known as the standard *Newton-Raphson* scheme. Theoretically, the Newton-Raphson scheme has *Quadratic convergence*. This means that the convergence rate of this scheme is proportional to the square of the number of iterations. This makes the Newton-Raphson method an efficient coupling scheme.

If the residual functions were to be known, the Jacobian for the function could be calculated, which would lead to faster convergence. But in practice, these functions are unknown, which makes it impossible to calculate the exact Jacobian. However, an approximate a Jacobian for the function can be calculated from the data available of previous iterations and time steps. This technique of calculating the approximate Jacobian to solve the function, is called the Quasi-Newton method.

Calculating the approximate Jacobian for a function from a set of data requires more computational work. This increases the cost of every iteration that is performed at each time step. Several methods have been developed for estimating the approximate Jacobian. Some of the most recent and state of the art methods would be introduced in this section.

The methods such as the IQN-ILS, MS-IQN-ILS, ML-IQN-ILS and the IQN-MVJ methods are recently developed methods which provide efficient ways of approximating a Jacobian.

3.5.1. IQN-ILS

The *Interface Quasi Newton- with estimation of Inverse Jacobian through Least Squared* method, is a state of the art second-order coupling method. As the name suggests the IQN-ILS method uses the least square method to estimate the inverse Jacobian. Although methodically different, the idea behind IQN-ILS method is similar to Broyden's method [6]. From equation 3.15 it is clear that, computing the inverse Jacobian of the function explicitly is not necessary. If the product of the residual $-R(p^k)$ and the inverse Jacobian $(\mathcal{J}^{-1})$ is calculated the problem should be solved.

To compute the inverse Jacobian through least squares, the data of the residuals r^k and the variables p^k from previous iterations need to be stored. The residual vectors would then be in the following manner,

$$r^k, r^{k-1}, \ldots, r^1, r^0 \tag{3.19}$$

for the corresponding values of p,

$$p^k, p^{k-1}, \ldots, p^1, p^0 \tag{3.20}$$

After each coupling iteration the difference of the residuals can be calculated and stored in another set of vectors,

$$\Delta r^{k-1} = r^k - r^{k-1} \tag{3.21}$$

$$\underline{V}^k = \begin{bmatrix} \Delta r^{k-1} & \Delta r^{k-2} & \ldots & \Delta r^1 & \Delta r^0 \end{bmatrix} \tag{3.22}$$

Information on the residual differences from the previous q time steps can also be re-used, to make the estimation more accurate.The matrices then would be given by,

$$V^k = \begin{bmatrix} \underline{V}^k & V^n & \ldots & V^{n-q+2} & V^{n-q+1} \end{bmatrix} \tag{3.23}$$

a similar matrix can be formed for corresponding values of p

$$W^k = \begin{bmatrix} \underline{W}^k & W^n & \dots & W^{n-q+2} & W^{n-q+1} \end{bmatrix} \tag{3.24}$$

the optimal values of q is problem dependent. The vector $\Delta r = 0 - r^k$ is approximated as a linear combination of the known Δr^i. Then,

$$\Delta r \approx V^k c^k \tag{3.25}$$

$$\therefore c^k = \left(V^{kT} V^k\right)^{-1} V^{kT} \Delta r \tag{3.26}$$

This implementation can get unstable if the number of columns in v are high. Therefore, it is safer to do a $Q - R$ decomposition of the matrix V such that,

$$V^k = Q^k R^k \tag{3.27}$$

where Q is an orthogonal matrix and R is an upper triangular matrix. Since, V is being updated every iteration, these matrices also have to be recalculated every iteration. then the set of vectors c^k can be calculated as follows,

$$R^k c^k = Q^{kT} \Delta r \tag{3.28}$$

the corresponding values of $\Delta\tilde{p}$ can be calculated as follows,

$$\Delta\tilde{p} = W^k c^k \tag{3.29}$$

from eq 3.15 and 3.29 we have,

$$\Delta r = \Delta\tilde{p} - \Delta p \tag{3.30}$$

$$\therefore \Delta p = W^k c^k - \Delta r \tag{3.31}$$

where $\Delta r = -r^k$. All this can be summed up into an algorithm to make the IQN-ILS coupling scheme. The memory usage of the IQN-ILS solver depends largely on the size of the matrix V^k. The greater the number of time-steps that are re-used, the more memory it requires.

Degroote [2][7], in his articles explains that the regular Gauss-Seidel scheme is unstable only for a certain fraction of Fourier modes depending on the boundary conditions and the time-step. Therefore, a fully accurate Jacobian is not required for the convergence of the coupling scheme. Therefore, The IQN-ILS method performs quite well when used to approximate the Jacobian.

3.5.2. ML-IQN-ILS

The *Multi-Level IQN -ILS* scheme is an improvement over the standard IQN-ILS technique explained in the previous section. The ML-IQN-ILS uses more than one grid level each with a different number of grid points. The coupled solution is first calculated on the coarser grid for a low-rank approximation of the Jacobian. Then using these approximations, the coupling iterations are performed on the finer grid. This is repeated till the solution of the finest grid level is achieved.

Finding the approximation on the coarser grids provides a preconditioning for the finer grid levels. This reduces the cost of computation of the Jacobian on the finer grids, increasing the convergence rates. In figure 3.5 this process can be clearly observed.

The coupling mesh at the interface of the two meshes remains the same and the interpolation between the fluid and solid grid is done accordingly. Therefore the Jacobian obtained from the coarser grid can be directly used in the the coupling algorithms in the finer grid without any mapping.

The ML-IQN-ILS method is an efficient method for solving strongly coupled problems. The CPU time required for convergence in this method is lower than than the regular IQN-ILS, due to the lower coupling time for the coarser grid, and the lower number of iterations required for the finer grid.

3.5.3. Manifold Mapping

In the article by Blom et al. [8], they have developed a method of mapping the solution from a coarse mesh to a fine mesh using manifold Mapping. Manifold mapping is chosen over other space mapping

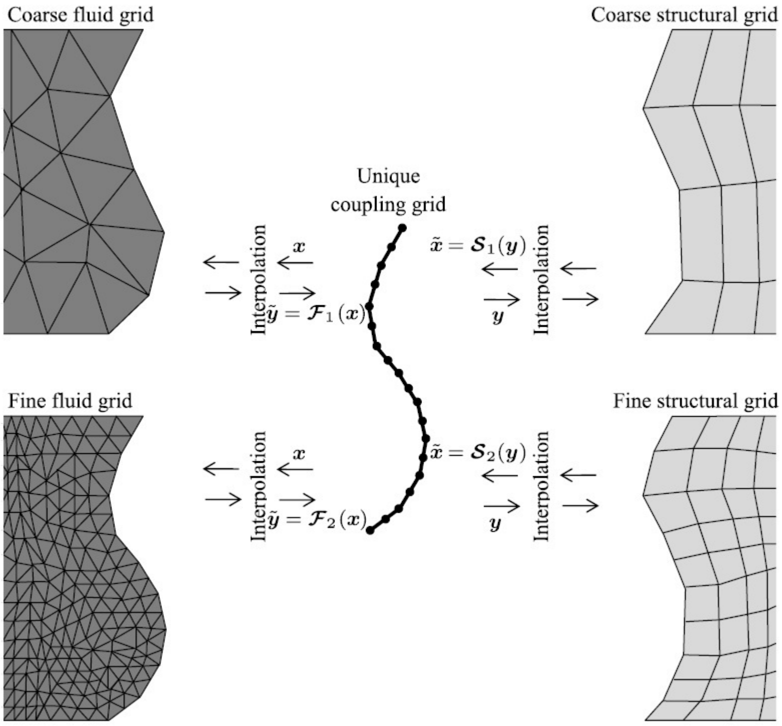

Figure 3.5: On the left side of the figure, the coarse and the fine fluid mesh of the fluid domain are shown, the corresponding coarse and the fine meshes of the solid are shown in the right side of the figure. The Multilevel IQN-ILS, first couples the coarse grid, then the Jacobian is passed on to a fine grid [2].

methods, since it has proven convergence to the right solution. This makes the technique robust to be used for Fluid structure problems.

This method makes use of minimization or optimization techniques to converge to a solution in the coarse mesh and then maps it on the finer mesh. In the article Blom [8] has compared this method to the IQN-ILS and other space mapping methods for a Benchmark test case by Turek and Hron [9], proving that the manifold mapping method reduces the time of convergence by 40%.

3.5.4. MVQN

The *Multi-Vector Quasi Newton* method is a state of the art method that has been presented in the article by Bogaers et al. [10]. The MVQN method estimates the approximate Jacobian for the Quasi-Newton method, which is updated at every iteration and contains the information of all the previous time-steps.

In this particular method, the Jacobian is first approximated using the generalised secant method, given by,

$$J_F^{n+1} \Delta D_F^{n+1} = \Delta F_F^{n+1} \tag{3.32}$$

where ΔD_F^{n+1} is the interface displacement vector and ΔD_F^{n+1} is the interface force vector. The subscript F signifies the fluid field variables.The approximation is made with the data from the first time-step. When information of the previous time-steps are used, the approximation is found to be better. This has been done in the LS method as discussed in 3.5.1. The information from previous time-steps can be reused to predict the Jacobian by LS which is defined by the user. The Multi-Vector update method however makes use of the information from multiple time steps without appending any additional information. The multi-vector update method works as follows,

$$J_{F,k+1}^{n+1} = \tilde{J}_{F,k+1}^{n+1} + J_F^n \tag{3.33}$$

where $\tilde{J}_{F,k+1}^{n+1}$ denotes the Jacobian update approximation. Therefore, a secant equation for $\tilde{J}_{F,k+1}^{n+1}$ can be constructed,

$$\tilde{J}_{F,k+1}^{n+1}\Delta D_F^{n+1} = \left(\Delta F_F^{n+1} - J_F^n \Delta D_F^{n+1}\right) \tag{3.34}$$

This method is similar to Broyden's method [6]. Bogaers [10] has compared the performance of this coupling scheme to other Quasi-Newton schemes and shown that the performance of the method is better than the IQN-ILS method by 40-50% when there is a reuse of 4 time-steps. The main remarks that have to be taken care of while using this method are,

- Remark 1: The convergence tolerance of the individual solvers have to be lower than the FSI coupling tolerance.
- Remark 2: The inverse of matrices is advised to be done by matrix factorization method rather than the standard inversion.
- Remark 3: The number of vectors in ΔD and ΔF should never exceed the number of DOFs.

Till now a complete list of coupling schemes has been put forward and it has also been observed that the higher order coupling schemes such the IQN-ILS, ML-IQN-ILS, Manifold Mapping and the MVQN are all capable of efficiently solving strong coupling problems. But the lower order schemes are also capable of solving strong coupling problems, when they are used with a pre-conditioner.

3.6. Simulating Turbulence Induced Vibrations through FSI

In the previous sections the state of the art coupling algorithms for partitioned solvers have been discussed. As already discussed before, partitioned solvers are the best suited methods for the current application. To simulate TIV, the FSI simulation is initiated by the fluid solver followed by the structural solver. The data calculated from the fluid solver are then mapped over the solid mesh spatially and then solved with a suitable temporal scheme. The displacement, velocity and the forces at the solid and fluid mesh interface, are taken as the key coupling parameters.

Since the application involves strongly coupled problems, more emphasis was given on implicit coupling methods. First-order coupling methods such as the Jacobi and the Gauss-Seidel coupling schemes were studied. Second-order Quasi-Newton methods like the IQN-ILS, ML-IQN-ILS and MVQN were also studied. Theoretically second-order coupling schemes are proven to be more stable and have higher convergence rates compared to first-order coupling method. Based on the ease of implementation two coupling methods were selected, namely the Gauss Seidel and the IQN-ILS coupling methods. Due to the simplicity of the code, the Gauss Seidel method is easy to implement and is proven to be capable for solving strongly coupled FSI problems. The Gauss Seidel scheme has been already implemented in the commercial package Star-CCM+. The IQN-ILS method has already been implemented in OpenFOAM. In Chapter 6, the performance of Gauss Seidel coupling scheme has also been validated for strongly coupled problems. The fluid and the solid solvers used are treated as black-box solvers solving the specific fluid and solid equations.

4

Turbulence Induced Vibrations

In the previous few chapters, an overview was provided on the classification of flow induced vibrations and how the simulations can be performed through fluid structure coupling. To initiate the vibrations on a structure, a proper fluid solver needs to be identified. Since the flow is turbulent in nature, the type of fluid solvers used can range from high fidelity solvers such as Direct Numerical Simulation (DNS) to low fidelity solvers such as RANS. But, before pitching into the topic of turbulence models , it is important to have a basic idea of turbulence. Turbulence in a literary sense means chaotic or random behaviour or in other words unpredictable in nature. However, is turbulence really unpredictable? Or is it possible to estimate the behaviour of the randomness? This chapter on turbulence will provide an insight into these questions and would try to shed some light on the characteristics of turbulent flows. With the help of statistics and other mathematical tools, it is possible to generate a mathematical model for turbulent flows, known as *Turbulence Model*. Further, in this chapter we would discuss the methods to model the random pressure fluctuations that are generated during a typical turbulent flow.

Turbulence is a random process, modelling turbulence accurately is dependent on the geometry and the flow of the fluid. Similar to the modelling of FIV, turbulence modelling also needs an in depth knowledge of the methods and the assumptions that are involved while modelling turbulence.

4.1. Turbulence - Order in Chaos

Turbulence may seem chaotic, but the statistical behaviour of a turbulent flow can be calculated. Involvement of statistics has improved the understanding of turbulence. Figures 4.1a and 4.1b from the book *An Album of Fluid Motion* [11] shows that the flow velocities and Reynolds number involved in these flows are very different from each other. Therefore, naturally one would expect a very different flow pattern. However, by visually looking at the wake region of these objects, it can clearly be seen that there are similarities between both flows.

It can be clearly observed that the large-scale vortex structures in both the flows here have the similar large scale geometry. After observing more closely the differences between the flows become evident at the smaller scales. This is also also observed in many other practical examples such as the jet flows or even wall bounded flows. This shows that turbulence although seemingly chaotic can be quantified in numbers and made deterministic. To discuss about turbulence in a more quantified manner a few terms need to be introduced to bring more clarity.

4.1.1. Energy cascade concept

In figure 4.1 it can be seen that the structure of turbulence is the same in both the sub-figures, even though the Reynolds number vary by orders of magnitude. Richardson [12] in his book introduces the concept of the energy cascade in turbulent flows, which is the base of all the turbulence models. According to this concept, the turbulent kinetic energy is created in the form of larger eddies, or the *macro-structure*, which are unstable (characterised by a large local Reynolds number). Later the unstable eddies break down into smaller eddies cascading (distributing) their energy. The smaller eddies keep on breaking down further into even smaller eddies till they dissipate (low Reynolds number). The

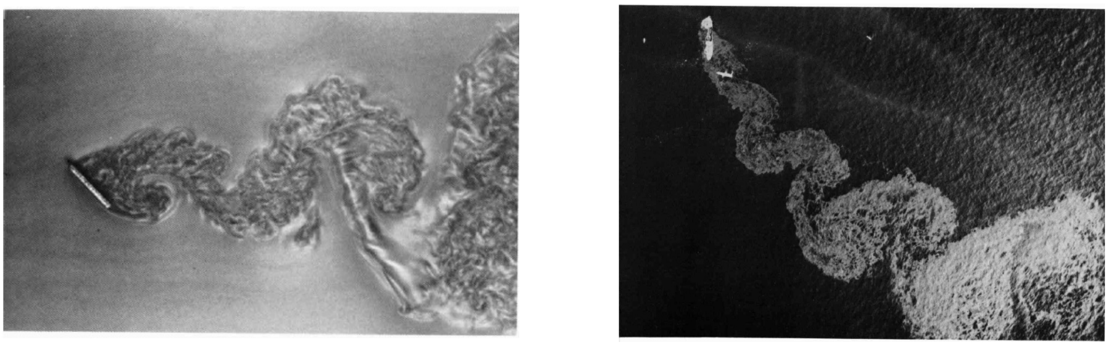

(a) Wake behind a plate at 45° angle of attack at a turbulent Reynolds number of 4300.

(b) Wake behind a grounded tankship at an angle of 45° at a Reynolds number of approximately 10^7.

Figure 4.1: Scale similarities between two different flows at different Reynolds number. The vortex formation in wake region of these objects can be clearly seen. The shapes of the large scale vortices in the wake region appear very similar.

turbulent kinetic energy is then dissipated due to the dominance of viscous forces. Figure 4.2 shows how a Reynolds number of eddies varies depending on the size of the eddies.

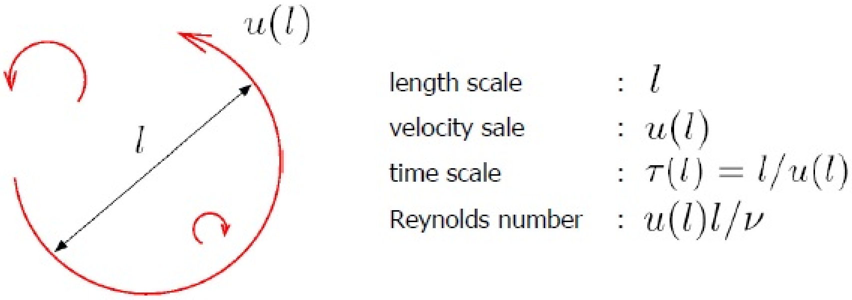

Figure 4.2: Calculation of Reynolds number of an eddy [13]. Here, l and u signify the length-scale and the velocity scale of the largest eddies.

The rate of this energy dissipation by viscosity (ϵ), is equal to the rate of energy transfer at large scales. This equation can be written down as

$$\epsilon \sim \frac{u_0^3}{l_0} \tag{4.1}$$

where, l_0 and u_0 are the length scales and velocity scales of the macro-structure. For smaller scales, energy dissipation rate is dominated by viscous dissipation. Therefore, the parameters involved in the same are the kinematic viscosity (ν) and the energy dissipation rate (ϵ). The smallest turbulent scales can be defined by these parameters. By equating the dimensions we can calculate the smallest scales, which were calculated by Kolmogorov in 1941, and are therefore known as Kolmogorov scales. These are given by

$$\eta = \left(\frac{\nu^3}{\epsilon}\right)^{1/4} \tag{4.2}$$

$$u_\eta = (\epsilon\nu)^{1/4} \tag{4.3}$$

$$\tau_\eta = \left(\frac{\nu}{\epsilon}\right)^{1/2} \tag{4.4}$$

where, η and u_η is the length scale and the velocity scale of the smallest eddies. τ_η is the time scale of the smallest eddies. The large eddies are commonly known as the *energy containing range*. The smallest eddies in the flow are known as the *dissipative range*. The range of eddy scales that are between these scales are known as the *inertial sub-range*. For the smallest eddy scales, viscous forces are dominant. Therefore, at the smallest scales Reynolds number is always $\ll 1$.

4.1.2. Statistical Approach to turbulence

A measured velocity signal at a certain point of a turbulent flow would be a stochastic signal. To analyse such fluctuating velocity and pressure signals, a statistical approach is necessary. Since these stochastic signals fluctuate about a mean value, an average of this signal can be obtained to define the flow for a statistically steady or an unsteady (time dependent) equation. The most commonly used averaging procedures are *Time averaging* and *Ensemble averaging*.

Time averaging, is when a stochastic signal is averaged with respect to a small duration of time. This expression can be written as,

$$\overline{u}^T = \frac{1}{T}\int_{+\frac{T}{2}}^{-\frac{T}{2}} u(t+\tau)d\tau \tag{4.5}$$

where T is the time interval considered for averaging. Apart from time averaging, *ensemble averaging* is another method for averaging. Ensemble averaging is the done with respect to the number of repeated samples taken of the same data. The sampling is done over multiple experiments. This can be written down as

$$\overline{u}^N = \frac{1}{N}\sum_{\alpha=1}^{N} u(\underline{x}, t; \alpha) \tag{4.6}$$

where N is the total number of samples considered. Both these averaging methods are well suited for defining a flow equation in their average sense. Henceforth, the averaging method which is used in this report would be the time averaged method. Turbulent flows consist of velocity fluctuations and average velocity. Once the average velocity of the flow has been calculated, the fluctuations in the velocity field and pressure can then be determined as follows,

$$u' = u - \overline{u} \tag{4.7}$$

$$p' = p - \overline{p} \tag{4.8}$$

where, u' and p' are the velocity and the pressure fluctuations for the turbulent flow at a given point. Since fluctuations are always taken about a mean value, an important property of these fluctuations comes into play. *The average of a fluctuating quantity is always equal to Zero*, which means $\overline{u'} = 0$ and $\overline{p'} = 0$. In later sections it will be clear that these averaging methods and properties can be used to model the turbulence from a standard Navier-Stokes Equation.

4.2. Turbulence Induced Vibrations

As discussed earlier, in Section 2.4, Turbulence Induced Vibrations are caused due to external excitation of the structural components due to random pressure fluctuations acting on the fluid-structure interface. The random pressure fluctuations are caused due to turbulent flow of the fluid around the structures. The effect of pressure fluctuations is more detrimental for axial flow across a closely packed fuel rod bundle in nuclear reactors. In such cases the forces exerted on the structure by the turbulent pressure and velocity fluctuations (p' & v') are more dominant.

Simulating TIV in a FSI simulation is possible if high fidelity fluid solvers, such as, LES or DNS are used. These fluid solvers do not average the pressure fluctuations. Hence, these can be mapped on the structural mesh, which generates a signal similar to that in TIV. In the following sections a more detailed explanation is given on why high fidelity models are better at simulating TIV as compared to low fidelity models such as RANS or URANS models.

4.3. Modelling Approach to calculate Turbulent quantities

Fluid motion is completely defined by the Navier-Stokes (NS) equations which are mainly the mass (continuity), momentum and energy balance equations. Due to the non-linearity of these equations, solving the Navier-Stokes equations analytically is very difficult; so much so that a prize money of a million-dollars has been announced for the one who solves the N-S equations. For now, the only known method to accurately and efficiently solve these equations for complex geometries and cases are by the use of numerical methods. In section 4.1.1 it has been seen that turbulent scales can vary in many orders of magnitude. The time and length scales of the largest eddies can range from kilometers to micro or nanometers. Computationally, this is a nightmare to solve. The computational power and memory requirement to solve the complete NS equations for a turbulent flow is significantly larger than a simple laminar flow. Although the computational power have been ever increasing, it is still not possible to economically solve the complete Navier-Stokes equations. Therefore, it becomes necessary to model the turbulence rather than solving using a brute force approach.

It becomes easier to study the behaviour of a turbulent flow through numerical methods. Current state of the art solvers can solve NS equations for turbulent flows in many ways. Some of the most important ones are the Direct Numerical Solvers(DNS), the Large Eddy Simulation (LES) and the Reynolds Averaged Navier Stokes (RANS) equations.

4.3.1. Direct Numerical Solver (DNS)

As the name suggests the Direct Numerical Solver uses the brute force method to resolve all the scales encountered in the turbulent flow. It involves solving the complete NS equations for all the scales involved in the flow. DNS is the most expensive, but also the most accurate way of solving the N-S equations. To get a proper solution, DNS demands high grid refinement, and Courant numbers as low as ≈ 0.01 to solve for the smallest eddy length scales (Kolmogorov scales). Since, there is no modelling involved, the velocities are directly calculated as stochastic signals rather than averaged values. This makes the solution of DNS to be ideal for simulating Turbulence Induced Vibrations, since the data obtained need not be post-processed and can be directly mapped and transferred to the solid solver. DNS is highly used in the fields of research to validate theories and for generating benchmark data for other studies. However, due to its high computational costs, DNS is uneconomical for most practical applications.

4.3.2. Large Eddy Simulations (LES)

Large Eddy Simulation or LES is a novel method that was first introduced in 1963 by Smagorinsky [14]. The idea behind the model is to solve the NS equations only for the largest of the eddies which the mesh grid is capable of resolving, and the rest of the smaller scales can be calculated using subgrid scale models. The order of the sub-grid filtering of the smaller scale eddies are calculated from the energy spectrum, where the smaller eddies become isotropic in nature. Smagorinsky [14] in his article gave his model for the smaller scale eddies and therefore, setting up the base for the LES models.

Although, LES is computationally more efficient than DNS, assumptions that are made during the modelling of the smaller scale eddies can lead to differences in results provided by LES, when compared to DNS. Moreover, when large or very complex geometries are involved, LES still is very expensive to compute. Similar to DNS, LES also solves the equations to obtain a stochastic signal for the velocities and pressures, therefore they can also be used in Fluid Structure interaction problems. For Nuclear reactor applications, the length scales of the complete fluid domain can be in the order of a few meters, which are very huge compared to standard CFD problems. Due to this reason the mesh size of the domain in case of LES can become very large. Therefore, a lot of time and memory is required to solve the problem. For most FSI cases LES is be an expensive option.

4.3.3. Reynolds Averaged Navier Stokes (RANS)

Reynolds Averaged Navier Stokes or RANS is another method to solve for NS equations for turbulent flows. Unlike the LES and the DNS methods, RANS models do not provide much data on the turbulent velocity or pressure fluctuations in the flow field, since they only calculate the average values of the velocity and the pressure fields. To get a better understanding, let us consider a NS equation for an incompressible turbulent flow. The continuity equation would be given by-

$$\frac{\partial u_i}{\partial x_i} = 0 \tag{4.9}$$

from eq 4.7 we know that

$$u_i = \overline{u_i} + u_i' \tag{4.10}$$

substituting eq 4.10 in eq 4.9 and averaging the whole equation w.r.t. time we get,

$$\frac{\partial \overline{u_i}}{\partial x} = 0 \tag{4.11}$$

This is the *Reynolds Averaged equation for continuity*. Similarly, the momentum equation for the incompressible flow is given by,

$$\frac{\partial u_i}{\partial t} + \frac{\partial u_i u_j}{\partial x_j} = \frac{\partial}{\partial x_j}\left[-\frac{1}{\rho}p\delta_{ij} + \nu\left(\frac{\partial u_i}{\partial x_j} + \frac{\partial u_j}{\partial x_i}\right)\right] \tag{4.12}$$

substituting eq 4.10 in eq 4.12 and averaging it we get,

$$\frac{\partial \overline{u_i}}{\partial t} + \frac{\partial \overline{u_i u_j}}{\partial x_j} = \frac{\partial}{\partial x_j}\left[-\frac{1}{\rho}\overline{p}\delta_{ij} - \overline{u_i' u_j'} - \nu\left(\frac{\partial \overline{u_i}}{\partial x_j} + \frac{\partial \overline{u_j}}{\partial x_i}\right)\right] \tag{4.13}$$

Eq 4.13 is the *Reynolds Averaged Momentum Equation*. When the eq 4.11 and eq 4.13 are analysed, it is seen that unlike the normal NS equations which had 4 equations and 4 unknowns, this particular set of equations has 6 equations and 11 unknowns. This creates a *closure problem*, where the number of unknowns are greater than the number of equations. Hence, to solve for all the unknowns more equations are necessary. The extra set of equations is provided by modelling the $\overline{u_i' u_j'}$ term in the eq 4.13. The $\rho\overline{u_i' u_j'}$ term in the equation is known as the *Reynolds Stress* also symbolized by τ_{ij}. One of the earliest models of the Reynolds Stress was provided by Boussinesq [15], known as the *Boussinesq approximation*. This model was key in development of many the turbulence models which are being used today in commercial and open-source CFD solvers. Popular turbulence models such as the $k - \epsilon$, $k - \omega$ and the $S - A,\ 1 - equation\ model$ are all based on the Boussinesq hypothesis.

Boussinesq Approximation

The Boussinesq approximation models the Reynolds Stress τ_{ij} as being proportional to the mean strain rate tensor (S_{ij}^*) and is written as follows,

$$\tau_{ij} = 2\rho\nu_t(S_{ij}^*) + \frac{2}{3}\rho K\delta_{ij} \tag{4.14}$$

$$\overline{u_i' u_j'} = \nu_t\left(\frac{\partial \overline{u_i}}{\partial x_j} + \frac{\partial \overline{u_j}}{\partial x_i}\right) + \frac{2}{3}K\delta_{ij} \tag{4.15}$$

where,δ_{ij} is the Kronecker Delta and K is the turbulent kinetic energy where

$$K = \frac{1}{2}\overline{u_k' u_k'} \tag{4.16}$$

another term which is required to be noticed here is ν_t. This term is known as the *Eddy Viscosity*. There are many methods which are used to model the eddy viscosity of a turbulent flow. The very first method was the Prandtl's mixing length hypothesis [15] which proposed that the eddy viscosity is proportional to the product of the square of the mixing length (l_m) and the velocity gradient in the wall normal direction,

$$\nu_t = l_m^2\left|\frac{\partial \overline{u}}{\partial y}\right| \tag{4.17}$$

The mixing length hypothesis solves the closure problem theoretically. This model is also known as a *Zero Equation Model*. But estimation of the mixing length is specific to the geometry and the type of flow. The $k - \epsilon$ model developed by Jones and Launder [16], was the first model which did not require a standard value for solving the equations. It solves for the transport equations of the turbulent kinetic energy (K) and the energy dissipation rate (ϵ). This property made the $k-\epsilon$ model popular to be used in commercial CFD packages. The eddy viscosity is then calculated using eq 4.18

$$\nu_t = C_\mu \frac{K^2}{\epsilon} \tag{4.18}$$

where $C_\mu = 0.09$ is a constant, the value of which has been experimentally determined. There are also other constants involved which are determined through experimental validation. The $k-\epsilon$ model is popular for high Reynold's number flows since it is robust. The downside of this model being that the prediction near the wall is not very good. This is usually compensated by usage of wall functions, which model the boundary layers. The $k-\omega$ model proposed by Wilcox [17], is an improvement over the standard $k-\epsilon$ model and does not require wall functions. The $k-\omega$ model is not suitable for geometries with sudden changes in gradients, such as sudden separation. The turbulent viscosity is modelled through $k-\omega$ model by,

$$\nu_t = C_\omega \frac{K}{\omega} \tag{4.19}$$

where, $\omega = \dfrac{\epsilon}{K}$

Since the $k-\epsilon$ and the $k-\omega$ models have two extra equations to solve (for k and ϵ or k and ω), these equations are also known as the *Two Equation Models*. Also there are other models which have been developed based on these two models like the $k-\epsilon\ RNG$ model and the $k-\omega\ SST$ model. These models try to eliminate a few of the problems that the standard models tend to face, making them more accurate.

The main disadvantage of the models based on Boussinesq approximation is that they assume turbulence to be isotropic in nature for all the length scales. This assumption is not true for many cases. In many simulations it is observed that these models over predict the values of turbulent kinetic energy in many regions or they tend to stabilize the results for an unsteady turbulent case when sudden changes in velocity gradients are observed.

Reynolds Stress Model

The Reynolds stress model solves the closure problem without the Boussinesq hypothesis. It does not consider the turbulence to be isotropic in nature, and therefore, is expected to give a more accurate result than the models based on the Boussinesq hypothesis. This model directly calculates the Reynolds stress from the transport equations. The method was first brought up by Launder [18] in 1975. This model involves calculating the Reynolds stress $\rho\overline{u_i'u_j'}$ from transport equations. The exact transport equations can be written as follows [19]:

$$\begin{aligned}
\frac{\partial}{\partial t}\left(\rho\overline{u_i'u_j'}\right) + \frac{\partial}{\partial x_k}\left(\rho u_k\overline{u_i'u_j'}\right) = &- \frac{\partial}{\partial x_k}\left[\rho\overline{u_k'u_i'u_j'} + \overline{p'\left(\delta_{kj}u_i' + \delta_{ik}u_j'\right)}\right] \\
&+ \frac{\partial}{\partial x_k}\left(\mu\frac{\partial}{\partial x_k}\overline{u_i'u_j'}\right) - \rho\left(\overline{u_i'u_k'}\frac{\partial u_j}{\partial x_k} + \overline{u_j'u_k'}\frac{\partial u_i}{\partial x_k}\right) \\
&- \rho\beta\left(g_i\overline{u_j'\theta} + g_j\overline{u_i'\theta}\right) + \overline{p'\left(\frac{\partial u_i'}{\partial x_j} + \frac{\partial u_j'}{\partial x_i}\right)} - 2\mu\overline{\frac{\partial u_i'}{\partial x_k}\frac{\partial u_j'}{\partial x_k}} \\
&- 2\rho\Omega_k\left(\overline{u_j'u_m'}\epsilon_{ikm} + \overline{u_i'u_m'}\epsilon_{jkm}\right) + S_{user}
\end{aligned} \tag{4.20}$$

which can be summarised to give the following equation,

$$\text{Local Time derivative} + C_{ij} = D_{T,ij} + D_{L,ij} + P_{ij} + G_{ij} + \phi_{ij} - \epsilon_{ij} + F_{ij} + \text{User-defined source term} \tag{4.21}$$

where, C_{ij} is the *Convection-term*, $D_{T,ij}$ is the *Turbulent-diffusion term* and $D_{L,ij}$ is the *Molecular-diffusion term*, P_{ij} is the *Production term*, G_{ij} is the *Buoyancy term*, ϕ_{ij} the *Pressure strain term*, ϵ_{ij} the *Dissipation term* and F_{ij} is the *Production due to rotation*.

Of these terms, $C_{ij}, D_{L,ij}, P_{ij}$ and F_{ij} do not need modelling, the remaining terms $D_{T,ij}, G_{ij}, \phi_{ij}$ and ϵ_{ij} require modelling to close all the set of equations involved. Each of the terms use different modeling approaches to close the equations. In total the Reynolds Shear Stress Model solves a set of 11 equations.

The Reynolds stress model has the following advantages over the models based on Boussinesq hypothesis,

- The models based on Boussinesq hypothesis assume the turbulence to be isotropic, whereas the Reynolds Stress models solves for all the components for transport of Reynolds stress.

On the downside, the model also has drawbacks,

- Compared to other turbulence models like $k-\epsilon$ or $k-\omega$, this model is significantly more expensive.
- Like every RANS models, it calculates the averaged values which does not simulate the actual turbulent condition for FSI problems.

In conclusion, RANS models are more efficient in terms of computational costs compared to LES or DNS models due to lower requirements of computational power and memory. But they compromise on the accuracy since, modelling of turbulence makes use of coefficients and physical assumptions such as isotropy which are specific only to some kind of flows. The accuracy can be increased in many cases by careful tuning of these models according to the flow. Moreover, RANS models calculate the time averaged values of turbulent flows (pressure and velocity). This information when used in FSI models does not provide accurate results, since they lack complete information of the pressure fluctuations on the solid and fluid interface, which might be the cause of instabilities. Since RANS models are efficient, it would be of great advantage if these models can be modified and made suitable for FSI simulations.

4.4. Applications of URANS models and FSI for simulating TIV

Unlike the standard RANS models which are steady state models, URANS (Unsteady Reynolds Averaged Navier Stokes) involves time dependent quantities for velocities and pressures. This means that the development of turbulent flow from its initial state can be observed. If the time steps in an URANS model are sufficiently small, the mean velocities would show a behaviour similar to velocity fluctuations which averages out as the simulation progresses. While simulating the development of a turbulent flow using URANS models, it can trigger instabilities which causes vibrations in structural components. But these vibrations do not provide sufficient data about the dynamic behaviour of the system. Therefore, an initial external excitation can give the necessary behaviour.

In an article by Ridder [20], the author has simulated an experiment performed by Chen and Wambsganss [21] of a turbulent flow of water, parallel to a brass rod, in an enclosed steel tube. An initial perturbation is given to the brass beam in the form of an initial displacement after which the beam is allowed to vibrate freely. The frequency of this vibration has been measured. The perturbation is provided by calculating each mode of the beam, and accordingly providing the initial displacements. Using this method, all the structural modes and the damping ratio of the beam within the fluid are calculated. The natural frequencies and damping ratios provide information on the added-mass effect of the fluid on the structure.

Ridder, used URANS $(k-\omega\ SST)$ models to simulate this behaviour with good accuracy in terms of natural frequency and damping ratio. He used URANS to calculate the natural frequencies of the induced vibrations due to turbulent flows. The domain of the simulation consists of a flexible beam of brass in turbulent flow of water. Figure 4.3 describes the domain of the experiment. The resulting frequencies were calculated after simulating this case as a standard FSI problem with an URANS model. The results are shown in Table 4.1.

Average water velocity $[m/s]$	**10**	**20**	**30**
Experimental natural frequency $[Hz]$	27.9	27.7	27.5
Computed results in the article [20] $[Hz]$	26.7	26.4	26.1
Experimental modal Damping ratio	0.013	0.021	0.030
Computed modal damping ratio [20]	0.015	0.024	0.032

Table 4.1: Table summarizing the results of the simulations carried out by Ridder [20]

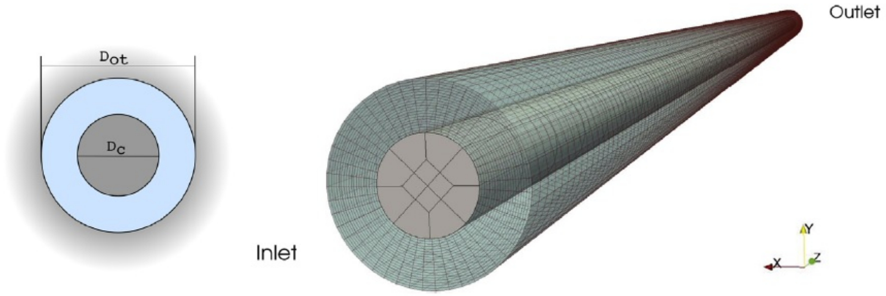

Figure 4.3: Domain of the Chen-Wambsganss experiment. The beam has fixed-fixed boundary condition (Dirichlet boundary conditions) at both the ends. $D_{ot} = 0.0254m$ and $D_c = 0.0127m$, the length of the domain $L = 1.19m$.

As shown in table 4.1, Ridder concludes that the natural vibration frequency of a solid beam in the turbulent flow can be captured by providing an external excitation. Ridder also tried to explain the discrepancies in the frequencies by trying to attain similar natural frequencies by applying a pre-stress to the beam in the lengthwise direction, increasing its natural frequency. More detailed analysis of this case will be covered again in Chapter 6. Similar results was also observed for another case study mentioned in the article by Ridder [20], involving a denser fluid and different boundary conditions.

However, the article [20] fails to answer several questions for instance,

- How the magnitude of initial perturbations are calculated.
- Does the perturbation taking into account the stability of the system
- How important is the role of the turbulence models that are chosen for the simulation.

The major drawback in the usage of URANS models is the lack of flow generated instabilities in parallel flow conditions due to absence of turbulent fluctuating fields $u_i' \& p'$. URANS models calculate time-averaged values for velocities and pressure, completely damping out the velocity fluctuations by the introduction of turbulent viscosity term (ν_t). The only information about turbulent fluctuations are available in terms of turbulent kinetic energy (k) and the energy dissipation rate (ϵ). In an FSI simulation, the k and ϵ quantities are not used when calculating the traction at the fluid-structure interface, rather only the time averaged quantities $\overline{p}$ and $\overline{u}$ are used due to which, the effect of turbulence is not taken into consideration. Therefore, these models are unable to simulate the instabilities that are caused by an actual flow. To solve this issue, a new approach would be discussed in Chapter 5, which can simulate the amplitudes of the vibrations with model which uses the turbulent quantities in URANS models.

In conclusion, it can be said that use of URANS in prediction of frequencies provides a good initial prediction on the system behaviour. It is possible to calculate to isolate each mode and therefore calculate the modal damping ratios more precisely. However, no comments can be made on the stability and the amplitudes of the system when using an external perturbation to stimulate the vibrations. To analyse this method, a complete study has been performed by comparing the computed frequencies with the experimental values in some other test cases in Chapter 6.

5

Modeling Pressure Fluctuations from Unsteady-RANS models

U-RANS models are widely popular in the industries as one of the cheapest and efficient ways of computing turbulent fluid flow properties. They employ a Reynolds averaging procedure to compute time averaged quantities of the flow such as velocity, pressure, and the temperature. The lower requirement of memory and computational power of these models make them ideal for computations involving large and complex geometries. Due to its averaging procedure, U-RANS models compute very little information on the fluctuating quantities $u_i' \& p'$ (refer equation 4.7 and equation 4.8) of a fluid flow. The computed data related to turbulent quantities are the turbulent kinetic energy (K), the energy dissipation rates (ϵ) and Reynolds shear stress tensor. Section 4.4 discussed about the study by De Ridder et al. [20] on ways to compute the dynamic properties of the structure by providing an initial perturbation or excitation to the solid. The perturbations were in the form of displacements to excite each mode of the structure to compute the natural frequencies and the damping ratios in the given flow characteristics. In a study by Eline et al. [22] they have used a similar concept to test the feasibility of U-RANS models by validating the results with experimental data.

The aforementioned studies involved an external excitation source which is provided as an initial condition. The modal frequencies and the damping ratios of the structure can be calculated from the resulting vibrations of the perturbation. However, the vibrations damp out when the flow reaches a steady state, and hence, the transition of the vibrations from an externally excited instability to a fluid-elastic instability cannot be simulated. Due to this, no information can be extracted on the critical velocities of the system, at which the system becomes unstable.

One approach to solve this issue is to model the turbulent pressure fluctuations from the mean flow quantities and later impose them on the solid. This would give an improved model to compute the dynamic properties of the structure and also the stability of the system. The K and ϵ values from U-RANS models estimate the turbulence in a given region of the fluid domain, but the values are time-averaged which are not used in simulations with fluid structure coupling. This chapter would discuss a new approach to model a turbulent pressure field from the K and ϵ values. The modeled turbulent pressure field, is mapped on to the fluid-structure interface to simulate TIV.

The first step in the modeling of the turbulent pressure field is to model the turbulent velocity field, which is later used to calculate the turbulent pressure field. A similar approach has also been used by Senthooran [23] in his work, where modeling of the velocity and pressure fluctuations were performed using the K and ϵ values from a RANS ($k-\epsilon$ Launder-Sharma) model. Figures 5.1 and 5.2 explain the difference between the working of a standard U-RANS model and the pressure fluctuation model. The pressure fluctuation model is an additional step that is applied to a standard U-RANS model. Every step involved in the modeling of pressure fluctuations will be explained in detail. For a better understanding of this model. It is advised to keep figure 5.2 as a reference while following the chapter.

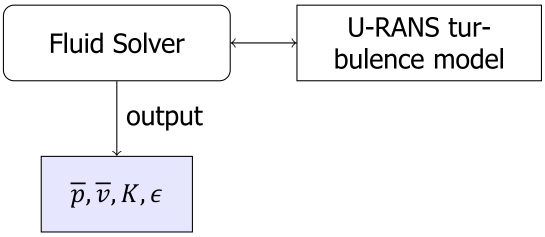

Figure 5.1: Flowchart depicting workflow of a standard flow solver with use of Unsteady-RANS model. The blue box indicates the output of the flow solver.

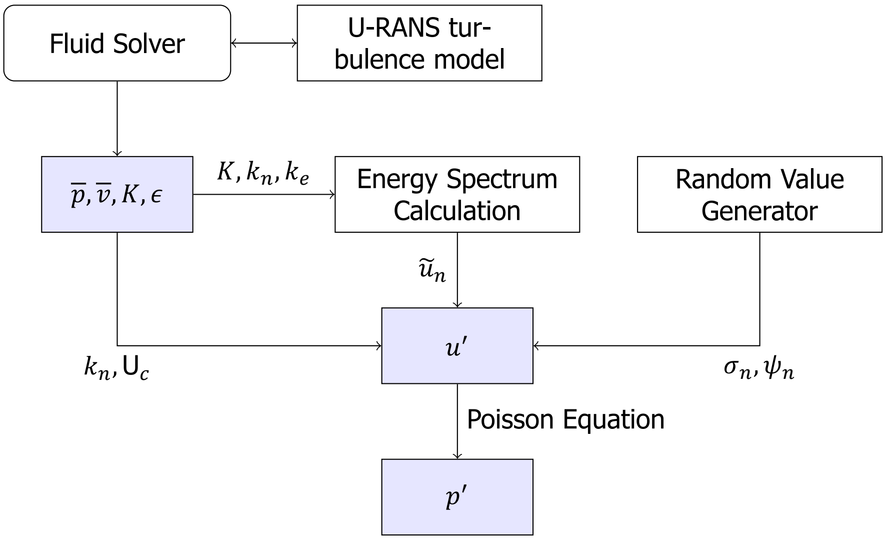

Figure 5.2: Flowchart depicting workflow of the flow solver with use of Pressure Fluctuation model. The blue boxes indicate the outputs of the flow solver.

5.1. Modeling the velocity fluctuations

The velocity fluctuations are modelled by expanding the function representing the velocity fluctuations with the use of Fourier series. The Fourier series is a good approximation of the velocity field due to its relation to the eddy length scales, and the periodic nature of the fluctuations. The velocity fluctuation field is modeled as a sum of velocity fluctuations caused due to all the eddy length scales, namely the largest eddy length scales to the Kolmogorov length scales. Since, the range of eddies in a turbulent regime is a continuous field, it is discretized into a selected number of modes or wave numbers. This is shown by

$$u'(\mathrm{x}, t) = \sum_{n=1}^{N} \widetilde{u}_n \cos[\mathrm{k}_n.(\mathrm{x} - t\mathrm{u}_c) + \psi_n + \omega_n t]\sigma_n \tag{5.1}$$

where $\widetilde{u}_n$, ψ_n, σ_n, ω_n and u_c are the amplitude, phase, unit direction vector of the n^{th} mode associated with the wave vector k_n, the characteristic angular frequency and the convection velocity respectively. The fluctuating velocity field can be modeled if all the unknown quantities can be calculated.

5.1.1. Calculating the wave vector and the direction vector

The wave vector (k_n) in a 1-dimensional sense is defined as the inverse of the eddy length scale. Since these eddies are in a 3-dimensional space, the wave number has to be mentioned in the form of a wave vector. Similarly, the direction vector (σ_n) of the velocity fluctuations is a unit vector which gives each component of velocity amplitude ($\widetilde{u}_n$) in a 3-dimensional space. Both these quantities namely, k_n & σ_n, are related to each other through the continuity equation.

For an incompressible flow, the continuity equation is given by equation 4.9, now applying equation 4.10 to the continuity equation, we get,

$$\frac{\partial \overline{u_i}}{\partial x_i} + \frac{\partial u_i'}{\partial x_i} = 0 \tag{5.2}$$

Subtracting equation 5.2 and equation 4.11 we get,

$$\frac{\partial u_i'}{\partial x_i} = 0 \tag{5.3}$$

to satisfy this condition we apply equation 5.3 to equation 5.1. We find that the necessary condition for satisfying both the equations is,

$$k_n.\sigma_n = 0, \text{ n = 1,...,N} \tag{5.4}$$

this implies that the wave vector k_n is orthogonal to the unit vector σ_n for any given mode. Assuming that the vector σ_n lies in a plane (k_1', k_2') which is perpendicular to the wave vector k_n. Then the coordinate transform between the components of vector k_n and the new coordinate system orthogonal to vector k_n would be,

$$\begin{bmatrix} k_1' \\ k_2' \\ k_3' \end{bmatrix} = \begin{bmatrix} \cos\phi_n & \sin\phi_n & 0 \\ -\cos\theta_n \sin\phi_n & \cos\theta_n \cos\phi_n & \sin\theta_n \\ \sin\theta_n \sin\phi_n & -\sin\theta_n \cos\phi_n & \cos\theta_n \end{bmatrix} \begin{bmatrix} k_1 \\ k_2 \\ k_3 \end{bmatrix} \tag{5.5}$$

where, ϕ_n, and θ_n are the polar angles of vector k_n. The unit vector σ_n can be expressed as,

$$\sigma_n = k_1' \cos\alpha_n + k_2' \sin\alpha_n \tag{5.6}$$

where α_n is the angle between k_1' and σ_n. By using equations 5.5, 5.6 and 5.4, we get the following expressions.

$$k_n = (\sin\theta_n \cos\phi_n) k_1 + (\sin\theta_n \sin\phi_n) k_2 + (\cos\theta_n) k_3 \tag{5.7}$$

$$\alpha_n = \tan^{-1}\left(-\frac{1}{\cos\theta_n} \right) \tag{5.8}$$

For simplicity, the turbulence is assumed to be *isotropic*. Therefore, an isotropic and homogeneous random field can be obtained by using probability density functions [23] for the random variables ϕ_n, ψ_n andθ_n,

$$\begin{aligned} \mathrm{P}(\phi_n) &= \frac{1}{2\pi} \\ \mathrm{P}(\psi_n) &= \frac{1}{\pi} \\ \mathrm{P}(\theta_n) &= \frac{1}{2}\sin(\theta_n) \end{aligned} \tag{5.9}$$

The probability density functions ensure isotropy with respect to wave vector k_n. The randomness of the fluctuating values is accomplished by employing a random value generator, to generate random values (X). These random values can be then used to calculate the values of ϕ_n, ψ_n and θ_n as a function of X and the use of the probability density functions in eq 5.9. The characteristic angular frequency ω_n is calculated by,

$$\omega_n = \epsilon^{1/3} k_n^{2/3} \tag{5.10}$$

5.1.2. Estimating the Energy Spectrum

The amplitude $\tilde{u}_n$ of the fluctuations, is a function of its wave number. The smaller wave numbers, in the range of k_l (the large eddy length scales) form the energy containing range. Therefore, the amplitudes of velocity fluctuations pertaining to this range of wave numbers are higher. In the inertial subrange the energy contained by each mode decreases proportional to $k^{-5/3}$ [15, 24]. Later for the

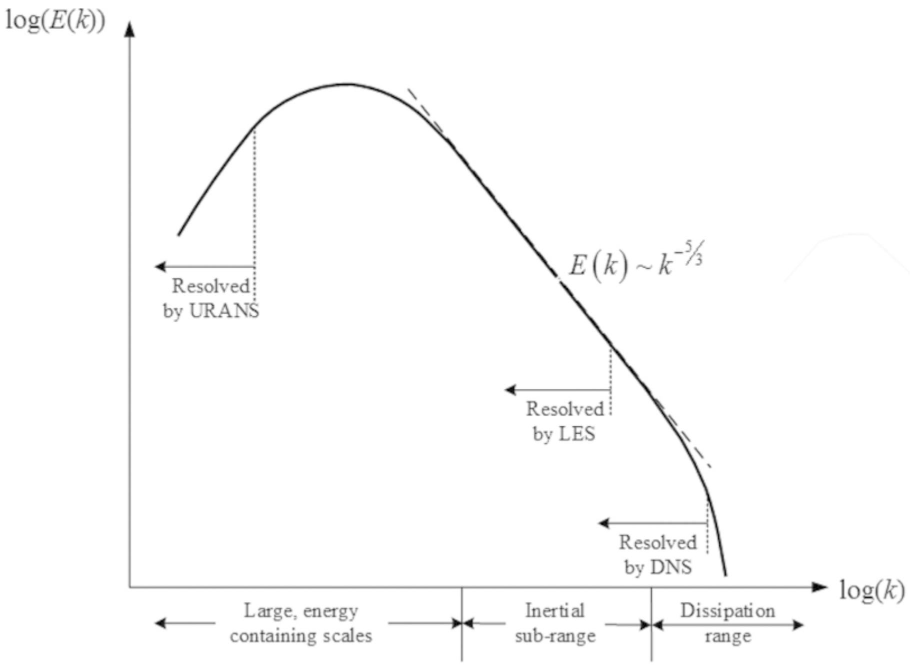

Figure 5.3: Typical energy spectrum for a turbulent flow plotted against wavenumber, k [25].

Kolmogorov wave numbers (k_N), the energy is the least. Hence, the amplitudes are calculated using the *Energy Spectrum* as a function of wave numbers and time. Von-Karman has suggested a model for calculation of the energy spectrum, $E(k,t)$, assuming local isotropy [24]. It is as follows,

$$E(k,t) = 2^{17/6}E(k_e)\frac{\left(k/k_e\right)^4}{\left[1+\left(k/k_e\right)^2\right]^{\frac{17}{6}}}\exp\left[-2\nu k^2\tau_\eta\right] \tag{5.11}$$

where τ_η is the Kolmogorov time scale for smallest eddies given by $\tau_\eta = \sqrt{\nu/\epsilon}$, k_e is the wavenumber where $E(k,t)$ is maximum, given by $E(k_e)$. It is the length scale at which contains the maximum energy. The variable t_0 is the initial time. The value $E(k_e)$ is approximated using the following equation [24],

$$E(k_e) = A\frac{2K}{3k_e} \tag{5.12}$$

where A is a constant of the order unity and K is the total turbulent kinetic energy. It is important to note that the estimation of energy spectrum in equation 5.11 is divided into 3 main regions. To get a better perspective also refer to figure 5.3

- *Energy containing range* : In the energy containing range the wave numbers are small, i.e. $k_l < k_e << k_N$. In this particular region the energy spectrum function ($E(k,t)$) is proportional to k^4 [24] which is clearly observed in equation 5.11. Also at smaller wave numbers the effect of viscosity is negligible, since the exponential term $\exp\left[-2\nu k(t-t_0)\right]$ becomes approximately equal to one for small wave numbers. Thus ignoring the effect of viscosity.
- *Inertial Sub-range* : According to Kolmogorov's theory, in the inertial subrange, i.e. $k_e << k_{inertial}$, the energy spectrum $E(k)$ is proportional to $k^{-5/3}$. In the equation 5.11, it can be observed that for $\frac{k}{k_e} >> 1$, the value of $E(k)$ becomes proportional to $\left(\frac{k}{ke}\right)^{-5/3}$.
- *Energy Dissipation range* : During the energy dissipation range ($k_e <<< k_N$), the viscosity effects become predominant and the energy contained is dissipated. Equation 5.11 tries to incorporate the effect of this in the term $\exp\left[-2\nu k^2\tau_\eta\right]$. In this region the value of $\left[-2\nu k^2\tau_\eta\right]$ becomes very large, therefore the value of the exponent term approaches zero.

The model of energy spectrum in equation 5.11 is more suitable for high Reynolds number flows, since at high Reynolds numbers, $k_N >> k_e$.

In the model for $E(k)$ given in equation 5.11, there are two unknowns (A and k_e) which are necessary to be calculated for the model to be used further.

Calculation of A and k_e

To calculate k_e and A, it is necessary to satisfy the basic definition of energy spectrum. Then using those conditions, the values of both the unknowns can be calculated. Now, in the inertial sub-range, the value of the energy spectrum is given by [24],

$$E(k_n) = A\epsilon^{2/3}(k_n)^{-5/3} \tag{5.13}$$

Since, viscosity effects are negligible in the inertial subrange, we can ignore the exponential term in the equation 5.11 and equating it to equation 5.13, we get,

$$A\epsilon^{2/3}k_e^{-5/3}\left(\frac{k_n}{k_e}\right)^{-5/3} = 2^{17/6}E(k_e)\frac{\left(k_n/k_e\right)^4}{\left[1+\left(k_n/k_e\right)^2\right]^{\frac{17}{6}}} \tag{5.14}$$

Also, in inertial sub-range $k_n/k_e >> 1$. By applying this condition and substituting the value of equation 5.12 in the above equation, we get

$$k_e = 2^{-17/4}\left(\frac{3}{2}\right)^{3/2}\frac{\epsilon}{K^{3/2}} \tag{5.15}$$

Therefore, by using the above equation, the first unknown k_e can be calculated. Now, by definition the turbulent kinetic energy can be calculated using the following equation,

$$K = \int_0^\infty E(k)\ \mathrm{d}k \tag{5.16}$$

Substituting equation 5.11 into equation 5.16, then dividing the equation by K,

$$\frac{2A\ 2^{17/6}}{3k_e}\int_0^\infty \frac{(k_n/k_e)^4}{[1+(k_n/k_e)^2]^{17/6}}\exp[-2\nu k\tau_\eta]\mathrm{d}k_n = 1 \tag{5.17}$$

Let, $k_n = k_e\tan(\xi)$ then we get,

$$\frac{2A\ 2^{17/6}}{3}\int_0^{\pi/2}\frac{\sin^4\xi}{\cos^{1/3}\xi}\exp[-2\nu k_e^2\tan^2\xi\ \tau_\eta]\mathrm{d}\xi = 1 \tag{5.18}$$

Now, substitute $\eta = \sin^2\xi$ and solve the above equation. We get,

$$\frac{2^{17/6}A}{3}\int_0^1 \frac{\eta^{3/2}}{(1-\eta)^{2/3}}\exp\left[-\beta\frac{\eta}{(1-\eta)}\tau_\eta\right]\mathrm{d}\eta = 1 \tag{5.19}$$

where, $\beta = 2\nu k_e^2$ Therefore, the value of A can be calculated using the following equation,

$$A = 3\left[2^{17/6}\int_0^1 \frac{\eta^{3/2}}{(1-\eta)^{2/3}}\exp\left[-\beta\frac{\eta}{(1-\eta)}\tau_\eta\right]\mathrm{d}\eta\right]^{-1} \tag{5.20}$$

Since, the value of k_e is known from equation 5.15,the value of A can be obtained from equation 5.20.

After the unknown parameters are computed, the value of $E(k_n)$ is computed for all the modes using equation 5.11. The number of modes has to be selected by the user depending on the resolution of the energy spectrum that is required. A higher number of modes gives a better approximation of the energy spectrum, however, it also increases the computational time required for its calculation.

5.1.3. Calculating the Amplitude

The amplitude $\tilde{u}_n$ defines the magnitude of fluctuation at each mode or wave number. To estimate the amplitude of each mode, we make use of the definitions of turbulent kinetic energy by equating the equations 5.1 and 5.16. In their discrete forms the equations would be as follows

$$\frac{3}{2}\sum_{j=k_l}^{k_N}\sum_{i=k_l}^{k_N}\tilde{u}_i\tilde{u}_j\cos\Theta_i\cos\Theta_j = \sum_{j=k_l}^{k_N} E(k_j)\delta k_j \tag{5.21}$$

where, $\Theta_n = \mathrm{k}_n.(\mathrm{x} - t\mathrm{u}_c) + \psi_n + \omega_n t$, and δk_j is given by,

$$\delta k_j = k_1(\exp[\Delta k] - 1)e^{[(j-1)\Delta k]} \text{ with,}$$
$$\Delta k = \frac{\log k_N - \log k_1}{N-1}$$

Now, from equation 5.21,

$$E(k_j)\delta k_j = \frac{3}{2}\tilde{u}_j\cos\Theta_j\sum_{i=k_l}^{k_N}\tilde{u}_i\cos\Theta_i \tag{5.22}$$

$$\frac{E(k_j)\delta k_j}{\cos\Theta_j} = \frac{3}{2}\tilde{u}_j\sum_{i=k_l}^{k_N}\tilde{u}_i\cos\Theta_i \tag{5.23}$$

squaring both sides,

$$\left[\frac{E(k_j)\delta k_j}{\cos\Theta_j}\right]^2 = \frac{9}{4}\tilde{u}_j^2\left[\sum_{i=k_l}^{k_N}\tilde{u}_i\cos\Theta_i\right]^2 \tag{5.24}$$

Substituting equation 4.16,

$$\left[\frac{E(k_j)\delta k_j}{\cos\Theta_j}\right]^2 = \frac{3}{2}\tilde{u}_j^2 K \tag{5.25}$$

Therefore, the amplitude of any mode, can be calculated using,

$$\tilde{u}_n = \frac{E(k_j)\delta k_j}{\cos\Theta_j}\left[\frac{2}{3K}\right]^{1/2} \tag{5.26}$$

From $\omega_n$and k_e the convective velocity is calculated by,

$$|\overline{u_c}| = \frac{\omega_n}{k_e} \tag{5.27}$$

$$\overline{u_c} = \frac{|\overline{u_c}|}{\sqrt{3}}[1 \quad 1 \quad 1] \tag{5.28}$$

with the calculation of u_c, all the ingredients required to calculate the turbulent velocity field have been calculated. Substituting all the calculated values in equation 5.1 the velocity fluctuation, u_n' can be calculated.

5.2. Calculating pressure fluctuation field

Since the velocity field has been computed, the next step of the model is to compute the pressure fluctuation field, p'. The pressure fluctuation is computed using the Poisson's equation [26]. To to derive the equation, we first consider the Navier-Stokes equation 4.12 and substitute equation 4.10. Therefore we get,

$$\frac{\partial(\overline{u_i}+u_i')}{\partial t}+\frac{\partial(\overline{u_i}+u_i')(\overline{u_j}+u_j')}{\partial x_j}=\frac{\partial}{\partial x_j}\left[-\frac{1}{\rho}(\overline{p}+p')\delta_{ij}+\nu\left(\frac{\partial(\overline{u_i}+u_i')}{\partial x_j}+\frac{\partial(\overline{u_j}+u_j')}{\partial x_i}\right)\right] \tag{5.29}$$

Then equation 5.29 is subtracted from the RANS momentum equation 4.13, to get the following equation,

$$\frac{\partial^2 p'}{\partial x_i \partial x_i}=-\rho\left[2\frac{\partial\overline{u_i}}{\partial x_j}\frac{\partial u_j'}{\partial x_i}+\frac{\partial^2}{\partial x_i \partial x_j}\left(u_i'u_j'-\overline{u_i'u_j'}\right)\right] \tag{5.30}$$

The method discussed above is most suited for 2-equation models, where the assumption of isotropy holds true. An important fact to note here is that the energy spectrum considered in this case is modelled using some standard models which are available to approximate the energy carried by the different length scales. There is a fair amount of flexibility on the type of model being used to best fit the amplitude of the velocity fluctuations.

Overall, this gives a good insight on the methods which can be employed to model pressure fluctuations from Unsteady-RANS models. For future work, this model can also be adopted for Reynolds Stress models, which would bring about all the properties required for generation of instabilities at the FSI interface without the assumption of isotropy.

5.3. Application of Pressure Fluctuation model in FSI

In section 4.4 it has already been discussed that simulation of TIV is not possible by a standard Unsteady-RANS model due to the absence of $u_i'\&p'$. However, if the pressure fluctuation model is applied to the solver, the pressure and velocity fluctuations in the field can also be calculated. Therefore, in case of an FSI simulation the pressure fluctuation model can be coupled to the solid solver. In this case the force acting at the fluid structure interface is taken as the summation of the forces exerted by the pressure fluctuations (p') and the time averaged pressure ($\overline{p}$). The pressure fluctuations act as an external excitation due to which the flow solver can induce TIV on the solid solver.

In an FSI simulation, the fluid solver takes the displacements and the velocities of the mesh interface as the input and gives the traction as its output. The traction is calculated using the mean pressure ($\overline{p}$), and the wall shear stress (τ). To employ the pressure fluctuation solver into the simulation, the calculated pressure fluctuations (p') would be added to the mean pressure, to get the total traction on the body due to pressure. This is given by,

$$Pressure\ Force=\int(\overline{p}+p')\ dA \tag{5.31}$$

This would ensure that the forces due to random pressure fluctuations are also transferred to the solid solver, leading to an external excitation condition. It is important to note that the mean pressure computed from the Unsteady-RANS model is not summed up to the modelled pressure fluctuation field while solving the fluid equations. The fluctuations are calculated as a post-processing method to the solver, with no direct interaction with the fluid solver.

5.4. Implementation of the Pressure Fluctuation model

The pressure fluctuation model which has been discussed in the current chapter has been implemented in the open-source CFD package OpenFOAM extend-3.2. The implementation required a detailed study of internal architecture of OpenFOAM. It was successfully achieved by writing the codes in various libraries and implementing the changes into a pre-existing solver. For this purpose the pimpleFoam unsteady solver was chosen. PimpleFoam solver is a widely utilised as a standard solver for unsteady simulations of turbulent flows. The detailed implementation of the code is provided in the Appendix of this report.

The modified pimpleFoam solver with the pressure fluctuation model is named as pimpleFluct. The same changes are also implemented in the FOAM-FSI solver, which is an FSI solver developed by David

S. Blom from TU Delft. The FOAM-FSI solver couples Deal.II [27], an open-source FEM library to OpenFOAM extend-3.2 which is a FV library. The pimpleFluct code is also incorporated into the FOAM-FSI solver giving it the capability to perform FSI simulations. All the FSI and fluid simulations performed in this report have been performed by the use of the pimpleFluct solver that has been implemented by me during the course of this thesis work.

6

Applications of URANS in FSI to simulate TIV

In the previous Chapters a lot has been discussed on the feasibility of URANS in simulating TIV. Till now, two main approaches were discussed on the application of URANS. The first approach was discussed in section 4.4, which computed the dynamic properties of the structure by providing an initial perturbation or excitation to the solid. The second approach was discussed in Chapter 5, which involved the modelling of the turbulent pressure fluctuations from the mean flow quantities and later impose them on the solid. In the current chapter both approaches are put to the test. The results are validated by comparing the results of an experimental case or comparing the results with other numerical benchmarks.

For the validation of the first approach, three test cases were chosen. All the three test cases are application based experimental cases; therefore a proper comparison of results is possible. The first case is a laminar case, which is aimed at testing the ability of the coupling method to solve strongly coupled problems. The second and the third cases are aimed at simulating the TIV and calculating the dynamic properties of the structure for nuclear reactor applications. URANS models were used in both the test cases.

To validate the second approach, first the model itself is validated by performing a simulation of a plane channel flow, for which DNS results are already available. The DNS database is was generated by Abe et al. [28] for cases with Re_τ 180, 395, and 640. The comparison between the DNS results and the modeled results shows the degree of inaccuracy that the model can generate. This would give an idea of the deviation that can be observed in the FSI simulation and whether the deviations are acceptable or not. Finally the model is tested by performing an FSI simulation on a modified case of a numerical benchmark case. The simulation is performed with standard URANS without modelling, and also performed with the use of the proposed pressure fluctuation model. The results of both the simulations are then compared.

6.1. Simulating TIV through an initial perturbation

The study is set to attain two main objectives. The first objective is to study the accuracy and efficiency of using FVM-FEM coupling and to validate the use of Gauss Seidel coupling scheme to solve strongly coupled FSI problems. To achieve the first objective, Vattenfall-I FSI test case [29] is performed with the aforementioned methods. The second objective of the study is to validate the use of URANS turbulence models to simulate flow induced vibrations, and to predict the dynamic behaviour of structure. To achieve the second objective, two test cases are performed, the Vattenfall-II test case by the Vattenfall Group in Sweden [30], and the experimental case by Chen and Wambsganns [21]. These test cases focus on simplistic models of fuel rods in nuclear reactors. Nuclear reactor applications are the main driving force behind the selection of the test cases.

6.1.1. Vattenfall Case-1

Vattenfall Research and Development in Sweden has performed an experiment where a vertical slender rod/beam with a roller boundary condition and a clamped side is displaced and then released, after which its vibrations and damping under the influence of the surrounding fluid are investigated by Vu and Truc [31]. Water is pumped in longitudinal direction of the beam through the channel. The bulk Reynolds number based on the bulk velocity and half channel height is maintained to $Re_b = 3600$, which is laminar in nature. The centre of the rod is given an initial displacement $\delta = 10\ mm$ after which it is released to vibrate freely. The displacement of the rod is measured using a laser. This case is well suited to test the influence of the added mass on the structure, refer figure 6.1.

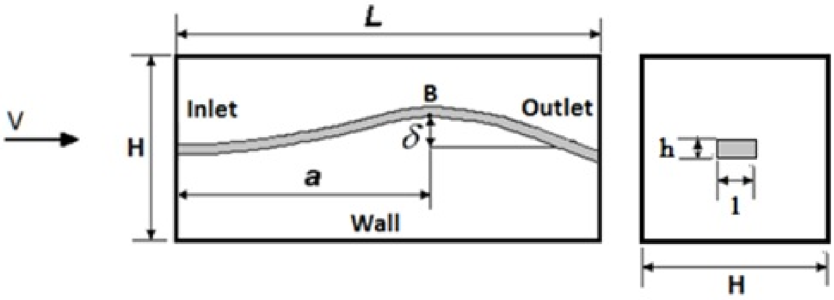

Figure 6.1: Domain of Vattenfall experiment [31]. Here, $L = 1.5\ m$, $H = 80\ mm$, $h = 8\ mm$ and $l = 20\ mm$. The fluid inlet velocity $v = 1\ m/s$ and the initial beam displacement at the center $\delta = 10\ mm$. The steel beam has a fixed - pinned boundary condition at the inlet and the outlet respectively. The flow is laminar in nature.

The stainless steel rod has a length of $L = 1.5\ m$, and a density of $\rho_{steel} = 8000\ kg/m^3$, a modulus of elasticity of $E = 193\ GPa$ and a moment of inertia, $I = 8.53 \times 10^{-10}\ m^4$. To ensure the use of correct boundary conditions for the beam in the simulations, an initial simulation was performed by vibrating the beam in vacuum (solid only simulation). The results of the simulation are compared to analytically calculated results. For a fixed-pinned beam, the following analytical model can be used to calculate the natural frequency of the first mode.

$$f = \frac{1}{2\pi}\left[\frac{15.418}{L^2}\right]\sqrt{\frac{EI}{\rho}}$$

where E is the Young's Modulus, I is the area moment of inertia, ρ is the mass per unit length and L is the length of the beam. The analytical approximation of the beam's natural frequency results in $12.37\ Hz$ for the first mode, which is in close agreement with the natural frequency of $12.34\ Hz$ calculated through the simulation. The density ratio ($\rho_{steel}/\rho_{water}$) for the experimental case is 8. A mesh and time convergence study is performed for the solid solver to check their influence on the final solution. The Gauss-Seidel coupling method (refer section 3.4) was employed using FEM-FVM coupling in STAR-CCM+. The FE discretization scheme is a numerical method for finding the approximate solution for a PDE (Partial Differential Equation) by dividing the domain into smaller elements. The structure equations are solved without segregation of its variables which is more efficient than FVM. However, FE discretization method is not conservative in nature. On the other hand, FV discretization schemes are conservative in nature, which reduces the number of equations required to solve in the case of fluid equations (Navier-Stokes equations). This makes FV methods an efficient method to use in fluid solvers. The case was simulated and then compared to the experimental results. Because the density ratios are comparable to the conditions in the nuclear reactors, the case would give an insight if the coupling scheme is stable for the given conditions.

Mesh and Time convergence study for the structural solver

The simulation with FE discretization for structural equations, is performed in STAR-CCM+. The mesh refinement was varied, from 100 to 650 divisions in the longitudinal direction. The effect of change in the mesh refinement on the calculation of modal frequency is observed in the Figure 6.2a.

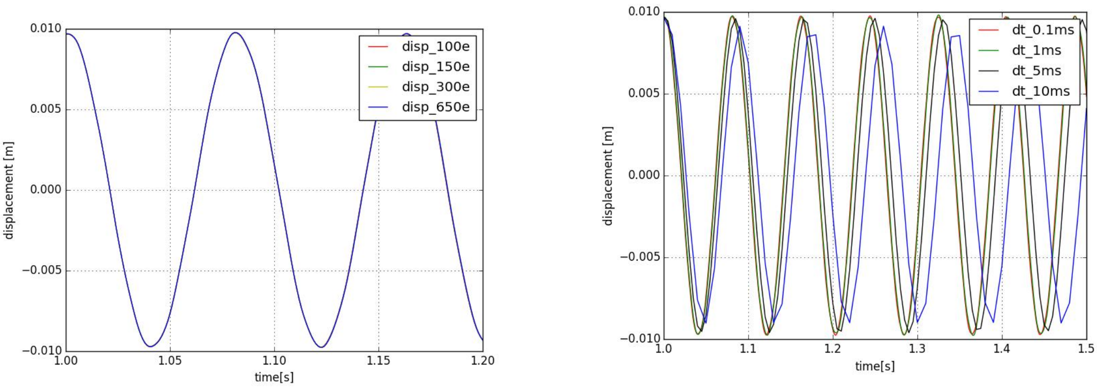

(a) Displacement of beam center vs Time graph showing the effect of mesh refinement on natural frequency.

(b) Displacement of beam center vs Time graph showing the effect of time step on the computed natural frequency of the solid beam.

Figure 6.2: Mesh convergence study with mesh refinement and time steps as the variables.

Case	Number of divisions	Frequency [Hz]
disp_100e	100	12.34
disp_150e	150	12.34
disp_300e	300	12.34
disp_650e	650	12.34

Table 6.1: Effect of mesh refinement on the calculated natural frequency of the beam through FE discretization method. It is observed that FEM discretization for structural solver is not sensitive to mesh refinement.

Table 6.2 compiles the results that were obtained during the study. A similar study was also performed by varying the time steps. The time steps for the simulation was varied from $0.1\ ms$ to $10\ ms$. The results have been shown in Figure 6.2b. Table 6.2 compiles the results that were obtained during the study.

From the study it can be observed that the mesh sensitivity of FE discretization method is negligible. The results virtually are not affected by the change in the number of mesh cells. In the time convergence study it was observed that the increasing the time steps lead to an increase in the % error of calculating the natural frequency. There was no significant numerical damping observed with the increase in time steps.

Eline et al. [22] has studied of the effect of mesh refinement and time steps on the calculated natural frequency by the use of FVM solvers. From the study it was observed that mesh refinement had a significant effect on the calculated natural frequency. An error as high as 64% was observed for a coarse mesh. From the time convergence study performed by Eline et al. for FVM, it was observed that the large time steps lead to significant numerical damping of the amplitudes. The damping effects decrease with use of smaller time steps.

From comparing the time convergence studies by Eline et al. [22] and the current study, it is observed that the FVM solvers are extremely mesh sensitive in comparison to FEM solvers. Also the time step used in case of the FEM solver was a 100 times larger than that used in FVM solver. FVM solver is also more sensitive to time steps used. In effect, the use of the FEM solver was found to be more over $10\times$ efficient than the use of the FVM solver for the solid solver.

FSI simulation setup, and Results

The FSI simulation was carried out in 3-D for both discretization schemes to get a better comparison of results with the experimental setup. The inlet velocity of the water is $1\ m/s$.

A fixed-pinned boundary condition is provided at the inlet and the outlets of the beam respectively. The solid beam is provided an initial displacement of $10\ mm$ at the center of the beam. This is carried out by applying an external force and carrying out a steady state simulation for the beam. Later, the force is removed to allow the beam to vibrate freely. The simulation is then coupled with the fluid

Result	Natural Frequency [Hz]	Error percentage
Analytical	12.37	–
dt_0.1ms	12.49	0.97
dt_1ms	12.26	0.89
dt_5ms	12.15	1.78
dt_10ms	11.76	4.93

Table 6.2: Effect of time-steps on the calculated natural frequency of the beam through FE discretization method. It is observed that increasing the time steps increases the error percentage of the estimation of natural frequency.

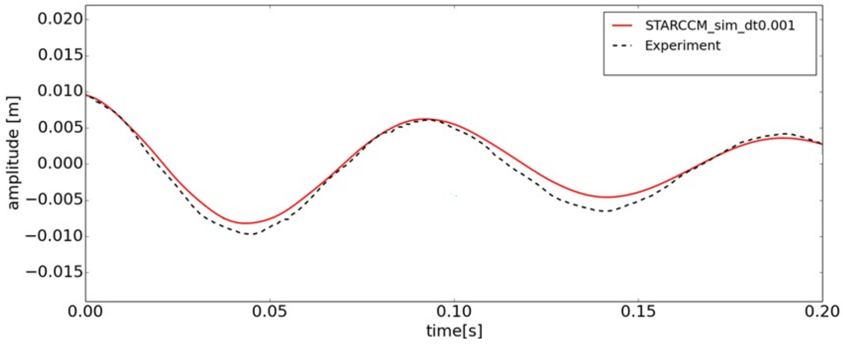

Figure 6.3: Comparison between displacements of the beam center in the experimental and simulation results as a function of time in the Vattenfall-I case study. The simulation results from STAR-CCM+ are close to the experimental values with an error percentage of 3.6%.

domain to replicate the conditions observed in the experiment. The simulation is carried out with FEM-FVM coupling. A hexahedral mesh is used for the fluid and the solid part. It is worth mentioning that for the fluid solver, a central differencing scheme with skew correction is used for the spatial discretization. A second order backward scheme is used as the temporal discretization for both the solvers with a time step of $1\ ms$. The Gauss-Seidel coupling scheme is used to couple the structure and the fluid solver. An average of 40 iterations was required to attain convergence of coupling iterations. The coupling scheme is therefore found to be stable for the current application.

The vibrations of the beam were seen to be damp due to the added-mass effect of water. The natural frequency of the beam was obtained by performing FFT (Fast Fourier Transforms) on the displacement signal obtained from the simulation. The response of the beam in comparison to the experimental measurements have been shown in Figures 6.3 and the results have been compiled in the Table 6.3. It's observed that the error percentage between the results is 3.6% which is within the acceptable error limit.

6.1.2. Vattenfall Case-2

The Vattenfall-II case is an application based case which involves simulation of vibrations induced on a steel rod due to turbulent flow of water around it. The experimental setup is shown in figure 6.4. The case simulates the vibrations on a fuel rod in a nuclear reactor surrounded by flow of turbulent water.

The length of the steel rod is $1.486\ m$ with a cylindrical cross-section. The outer diameter of the tube, $D_o = 8\ mm$ with a thickness of, $t = 0.6\ mm$. The inlet side of the tube is fixed (Zero displacement and no rotation) and of the outlet side the tube is pinned (zero displacement, but free to rotate in transverse direction). The domain consists of a wide inlet followed by a sudden constriction of the cross-sectional area. The sudden decrease in the area of the fluid flow leads to a turbulent flow in the water. The constricted area again opens up into a wide area. The mass flow rate of water is $10\ kg/s$. Using the hydraulic diameter as the length scale, the Bulk Reynolds number for the flow is calculated to be $Re_b \approx 1.2 \times 10^6$ which falls in the turbulent regime. The pressure fluctuations due to the turbulent flow around the tube results in vibrations of the steel tube. This simulation aims to capture the dynamic behavior of the steel tube in the given conditions and to compare it with the experimental results.

It can be observed for a fact that for large domains like the case of Vattenfall-II, to perform an LES,

Result	**Natural Frequency** (Hz)	**error** %
Experiment result	10.57	–
Eline et al. [22] (FVM-FVM)	11.21	7.68
Simulation result (FEM-FVM)	10.96	3.6

Table 6.3: Comparison between experimental values and simulated results of Vattenfall-I case study.

the number of cells required is in the order of 10^7 cells. This increases the computational costs of the simulation. Therefore, the use of U-RANS models is being validated in this particular case study. The main objective of this current study is to test the effect of different turbulence models on the dynamic behaviour of the structure.

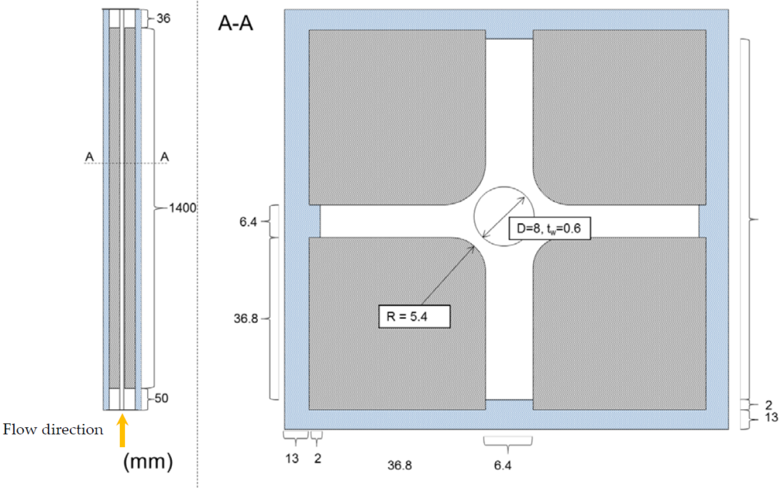

Figure 6.4: Domain of Vattenfall experiment case-2. The dimensions shown in the figure are in mm. The blue box in the figure is the external box of the experimental setup, and the grey regions are solid blocks to constrict the flow of water and generate turbulence. The fluid (water) is flowing in the confined white region within the blue box. The tube (beam) is shown as the circle in the center of the white region (fluid domain). The tube at the inlet side is fixed and pinned at the outlet.

Simulation set-up

In the framework of this test case, an assessment with two URANS models is performed. The models used were the $k - \omega\ SST$ and the RSM (Reynolds Shear-stress Model). The two models present two different assumptions for turbulence, the former assumes the isotropic condition, and the latter assumes the anisotropic behaviour of turbulence. We will compare the variation in the results for the two turbulence models with respect to experimental measurements by the Vattenfall Research and Development, Sweden [30]. The density ratio of the present configuration $\rho_s/\rho_f = 8$. A time step of $1 \times 10^{-3}\ s$ was used to simulate the case, with a hexahedral trimmed mesh for the fluid and a hexahedral mesh for the structure. A second order temporal scheme was used during the simulation. The first cell thickness of the mesh has a wall $y^+ \leq 5$. The simulation considers a FE discretization for the structure solver and FV for the fluid solver. Similar to the previous case, the Gauss Seidel coupling algorithm was used to couple the two solvers. Table 6.4 gives the exact specifications of the material properties which were used in the experiment. The initial perturbation provided in this case is imposed in form of a uniform body force, which is applied initially and then removed. The sudden removal of the force triggers the vibrations. Due to the uniform loading, mainly the first mode of the tube is excited.

Results and Discussions

Table 6.5 compiles the experimental the simulation results of this case. The displacements from the vibration of the beam were measured in two directions of the Cartesian coordinates (x and y) forming the cross sectional plane of the domain. The natural frequency of the vibration was calculated by performing FFT (Fast Fourier Transforms) of the displacement signal in both the directions. As it can be observed, URANS is capable of predicting the natural frequencies of the vibrating tube in a turbulent

Fluid Properties (Water)	
Density (ρ_f)	$1000\ kg/m^3$
Kinematic Viscosity (ν_f)	$1 \times 10^{-6}\ m^2/s$
Turbulent Intensity at inlet	1%
Structural Properties (Steel)	
Density (ρ_s)	$8055\ kg/m^3$
Elasticity Modulus	$193\ GPa$
Poisson Ratio	0.285

Table 6.4: Material properties in the Vattenfall case-II experiment.

flow close to the experimental results. The behaviour of a solid tube in case of URANS resembles that of a freely vibrating beam. The cases when performed using URANS leads to a high initial displacement of the tube which eventually damps out and reaches a steady state. Whereas, in the experimental case the vibrations are self sustaining in nature. Hence, the critical flow velocities (refer section 2.4) for TIV cannot be accurately predicted using this flow solver.

An important fact to observe is that the simulation of vibrations by providing an initial perturbation is not self-sustaining and vibrations are eventually damped out due to the added-mass effect.

Results	**Inlet volume flow rate** $[l/s]$	**Modal frequency (first mode)** $[Hz]$	
		X-dir	Y-dir
Experiment results	10	8.29	9.52
$k - \omega\ SST$	10	9.67	9.96
RSM	10	9.93	9.96

Table 6.5: Comparison table of the results between the simulations for Vattenfall case-2 experiment. It is seen that the change in the turbulence model does not have any effect on the behaviour of the beam. Also the calculated frequency is similar for X and Y-directions.

The comparison table 6.5 shows the results obtained from each of the simulations. It can be observed in the table that the frequencies in the x-direction and the y-direction are similar each other. Moreover, the x-direction frequency deviates from the experimental results by approximately 10%. In the y-direction however, the frequency prediction is more accurate. The first reason for the difference from the experimental results is the geometry. Since the geometry of the cross-section is symmetric about the X and the Y-axis, the modal frequency of structure in both the directions would be expected to be the same. The second reason of the errors may be due to non conformal meshes. Non conformal meshes usually involve errors in the mapping of data between the meshes. These errors can significantly influence the mapping of forces from the fluid to the structure domain therefore causing the deviations. Moreover, RANS models are unable to calculate pressure fluctuations at the interface. The simulated vibrations are not self sustained, which affects the dynamics significantly.

The second observation to be noted in the results is that the modal frequencies obtained from the structure solver are not directly dependent on the type of URANS model used. The $k - \omega\ SST$ model is based on the Boussinesq approximation of isotropic turbulence, and the Reynolds Shear Stress model (RSM) is based on calculating the turbulent quantities using transport equations for the Reynolds stress. Both the models eventually produced similar results. This fact leads to a conclusion that the calculations of time or ensemble averaged turbulent values do not have a direct role to play in FSI simulations. The main values used for the FSI simulation are the time averaged quantities of pressure ($\overline{p}$), calculated from RANS equations.

6.1.3. Flexible brass beam in turbulent water

Flexible beam in turbulent water flow is an experimental case by Chen and Wambsganns [21]. The case involves an annular flow domain along a cylindrical brass beam. The hydraulic diameter of the fluid domain is $D_h = 0.0127\ m$. The outer-wall is a rigid steel cylinder, the natural frequencies and the damping ratios are then measured for three constant inlet velocity conditions, $10\ m/s$, $20\ m/s$ and

30 m/s. The bulk Reynolds number for the flows can be calculated using

$$Re_b = \frac{uD_h}{\nu_f}$$

The Re_b for $u = 10\ m/s$ is calculated to be 1.21×10^6 which is in the turbulent regime. The beam is clamped (fixed) on both the ends. The beam has a core diameter of $D_c = 0.0127\ m$ and the annulus has an outer diameter of, $D_o = 0.0254\ m$. The length of the cylinder is $L = 1.19\ m$. The geometry of the domain can be visualised in Figure 6.5. The main objective of the test case is to investigate the effect of flow rate on the natural frequency of the structure. For this case, three inlet velocities are used, $10\ m/s,\ 20\ m/s$ and $30\ m/s$.

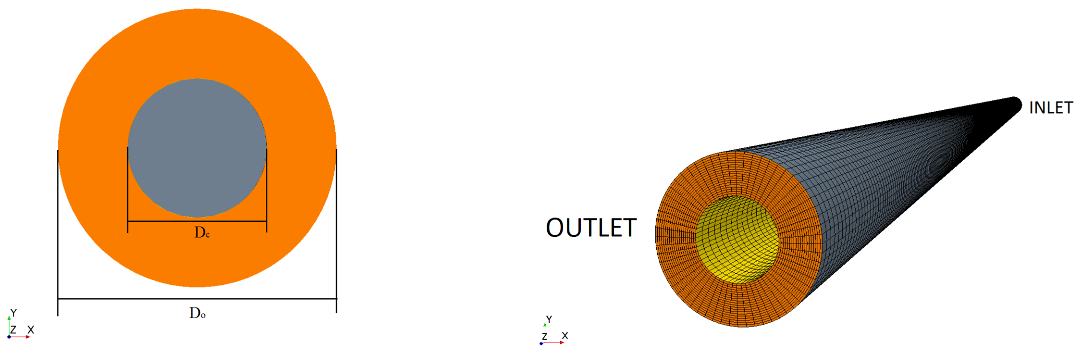

(a)

(b)

Figure 6.5: Geometry of the domain for the flexible brass beam in water experiment. The domain length $L = 1.19\ m$. The outer diameter $D_o = 0.0254$, and the inner diameter $D_c = 0.0127\ m$. The solid brass rod in fixed on both the sides.

Fluid Properties (Water)	
Density (ρ_f)	$1000\ kg/m^3$
Kinematic Viscosity (ν_f)	$1 \times 10^{-6}\ m^2/s$
Structural Properties (Brass)	
Density (ρ_s)	$8400\ kg/m^3$
Elasticity Modulus	$107\ GPa$
Poisson Ratio	0.331

Table 6.6: Material properties used in flexible beam in water experiment.

	Natural Frequency [Hz]		
Velocity	10 m/s	20 m/s	30 m/s
Experimental [21]	27.9	27.7	27.5
Computed	25.9	25.5	25.0
	Modal Damping Ratio		
Velocity	10 m/s	20 m/s	30 m/s
Experimental [21]	0.013	0.021	0.030
Computed	0.018	0.022	0.031

Table 6.7: Compiled results for experimental results and the simulated results. The frequencies of vibrations are seen to increase with the flow velocity. However, the damping ratio decreases linearly with an increase in the flow velocity.

Simulation Set-up

The FSI simulation was performed with water inlet velocities $10\ m/s,\ 20\ m/s$ and $30\ m/s$. The $k - \omega\ SST$ turbulence model was used for the three inlet conditions. The turbulence intensity at the

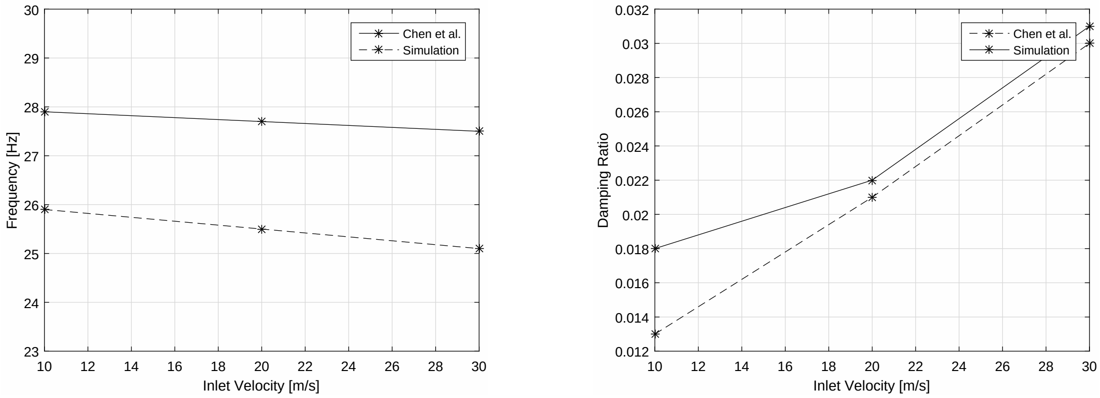

(a) Frequency Vs Velocity Plot

(b) Damping Ratio Vs Velocity Plot

Figure 6.6: Plots comparing the results obtained from experimental and simulation values. The plots depict the change of the natural frequency and the damping ratio of the brass beam as a function of flow velocity.

inlet of the domain is set to 5% with a turbulent length scale of $0.1\ cm$. The material properties of fluid and the structure are shown in Table 6.6. A hexahedral mesh is used to mesh the fluid and the solid domains. The first cell thickness of the wall $y^+ \geq 30$. Since the first cell of the mesh is in the log layer, y^+ treatment (wall functions) were used for the fluid domain. The density ratio of the present configuration $\rho_s/\rho_f = 8.4$. A time step of $1 \times 10^{-3}\ s$ was used to simulate the case. A second order temporal scheme was used during the simulation. Similar to the Test Case II, the structure solver used FE discretization, and the fluid solver used FV discretization scheme. The Gauss Seidel coupling scheme is used as the coupling algorithm.

An impulse force of $0.2\ m/s^2$ was applied for a period of $0.1\ s$, at a central patch of the beam. The impulse force has a Gaussian distribution curve as a function of time. The vibrations imposed due to the impulse force were analyzed using FFT (Fast Fourier Transforms). The damping ratios of the beam were calculated using a least square method. The simulation was performed till a steady state was of the solid was attained.

Results and Discussion

Initial simulation of a freely vibrating beam in vacuum was performed to calculate its natural frequency. The natural frequency of the beam in vacuum was calculated to be $28.49\ Hz$ analytically and $28.57\ Hz$ through simulation. The experimental measurements [21] show that the beam had a natural frequency of $28\ Hz$ in quiescent water. A simulation in quiescent water with similar boundary conditions was performed, and the frequency was calculated to be $26\ Hz$. This suggests that the boundary conditions of the beam in simulation do not completely match the boundary conditions of the beam in the experiment. A higher frequency of the beam is possible if the structure is pre-stressed. However, the paper by Chen and Wambsganns [21] does not mention any changes related to boundary conditions, therefore, a deviation in the results of about 10% can be observed. Figure 6.6 and table 6.7 show a comparison and the trend of the frequencies obtained as a function of velocity.

It can be observed that the natural frequency of vibration decreases by $0.4\ Hz$, as the average velocity increases by $10\ m/s$. The similar trend has also been observed in the experimental results for natural frequencies. Damping ratios in both the cases are a linear function of the flow velocity.

6.2. Simulating TIV through Pressure Fluctuation modelling

The second study is performed to validate the pressure fluctuation model which has been derived in Chapter 5. The study involves two test cases; the first case is a fluid only simulation to validate the results of pressure fluctuation model with DNS results. For this a DNS of turbulent plane channel flow was chosen.

After the case is validated, the second case is performed, which is a coupled FSI case. The FSI case is a numerical test case which is performed to check whether the fluid solver can generate TIV on the solid body. The results of this case are compared to a standard U-RANS model ($k-\omega$).

6.2.1. Plane Channel Flow test case

The turbulent plane channel flow is a widely researched upon numerical and experimental case. This case provides a lot of information on turbulent flows, instability and their mechanisms. A DNS test case performed by Abe et al. [28] of a turbulent plane channel flow case was chosen for this case. A picture of the mesh and the domain dimensions of the fluid domain are shown in figure 6.7. The flow has a friction Reynolds number, $Re_\tau = 640$. To simulate the case, the standard $k-\omega$ turbulence model was used with the pressure fluctuation model. The resulting pressure fluctuation field is later analysed and compared to the DNS database.

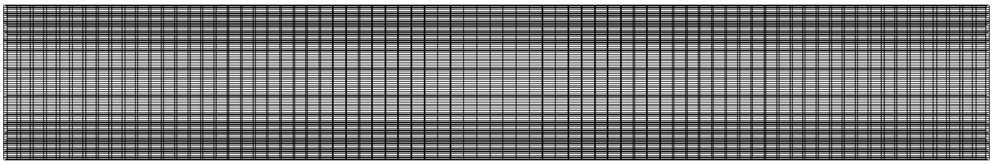

Figure 6.7: Fluid domain for turbulent plane channel flow. The length of the domain, $L = 12.75\delta$, and $H = 2\delta$. Here δ is the half channel height.

Simulation set-up

The plane channel flow simulation is performed in the CFD package OpenFOAM extend-3.2. The inlet and the outlet of the domain were given a cyclic boundary condition. The flow was forced by applying an external pressure gradient with a first order time stepping scheme, and the results were then compared after a steady state was achieved. The simulation was performed for a total time of 150 seconds, for the flow to reach a stable state. The time step utilized in was $1\ ms$. The flow was performed with standard $k-\omega$ model, without the use of wall functions for the mean velocities $\overline{u}$. A forcing term is used to let the flow accelerate to the required Re_τ. The forcing term was calculated from the definition of u_τ.

$$u_\tau = \left[\frac{\tau_{wall}}{\rho_f}\right]^{1/2}$$

where, u_τ is the friction velocity and T_{wall}, the wall shear stress. Since this is a 2-Dimensional simulation, a hexahedral mesh with a single cell thickness in the Z-direction. The first cell thickness used with a wall $y^+ \leq 5$.

The set-up of the pressure fluctuation model requires input of some parameters such as, the number of modes ($nModes$), the integration constant for η($intConst$)(refer equation 5.20 for η) , and the time at which the pressure model will begin to calculate the turbulent fluctuation fields ($stabTime$). The values of $50,\ 1000,$ and $80\ s$ were provided to each of the parameters respectively. The value of $stabTime$ is chosen to ensure that the calculations for pressure fluctuations are started only after the flow is developed; this ensures stability of the solver. The results from the simulations are compared to the results in the article by Abe et al. [28]. The results have been compared at the two different positions in the wall normal direction at a length of 6.375δ from the left end of the domain.

- Near the bottom Wall $y^+ \approx 4$(Point A).
- At the centre of the channel (Point B).

Results and Discussions

Figure 6.8a and figure 6.8b show the pressure fluctuations and the velocity fluctuations that have been modelled from the turbulence models for the complete domain. Similarly, the pressure and velocity fluctuations for all the components at Point B (half channel height), have also been shown in figures 6.9.

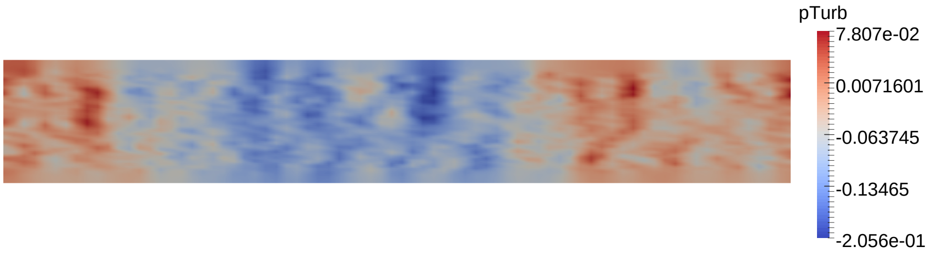

(a) Modeled pressure fluctuations from turbulence model.

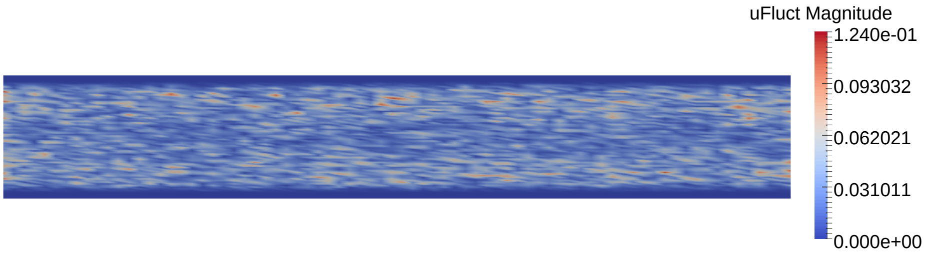

(b) Modeled velocity fluctuations from turbulence model.

Figure 6.8: Instantaneous picture of the modeled turbulent quantities through the pressure fluctuation model. The quantities of the pressure p' and velocity field u' are not scaled, they have units m^2/s^2 and m/s respectively.

It can be observed from the figures and the graphs that the velocity and the pressure fluctuations show a random behaviour. Achievement of the random behaviour in the flow was the first objective of the pressure fluctuation modelling. The second objective of the study was to determine whether the values of pressure fluctuations that are modeled using this method are comparable to the DNS results.

To analyze the modeled pressure fluctuations, a spectral analysis of the turbulent pressure field by taking the complete time signal at $y^+ = 10$ was performed. The resulting power spectrum is compared to results from the DNS database of Abe et al. [28]. Figure 6.10 shows the power spectrum of the turbulent pressure field p' signal. Looking at the figure, the power spectrum of the modelled pressure fluctuations can be divided into two main regions.

- The first region is the power spectrum in the range $10^{-1} \leq k\delta \leq 10^2$. In this range it can be very clearly observed that the power spectrum from the modelled pressure fluctuations is very similar to the power spectrum from the DNS database. This range of k is the energy containing range and contribute majorly to the magnitude of the pressure fluctuations.
- The second region is the power spectrum of the modelled pressure fluctuations in the range $k\delta > 10^2$. In this region, it is observed that the spectrum is greatly overestimated when compared to the DNS database. This region consists of smaller length scale eddies which contribute very little towards the energy contained by the turbulent pressure fluctuations.

Due to the direct dependence of pressure fluctuations calculated on the energy spectrum model (refer equation 5.11), it can be concluded that in the first region of the energy spectrum model provides a good estimate. This region mainly consists of the the larger eddy scales and inertial subrange ($k \approx k_e << k_{kol}$). However, in the deviation the in the second region suggests that the energy

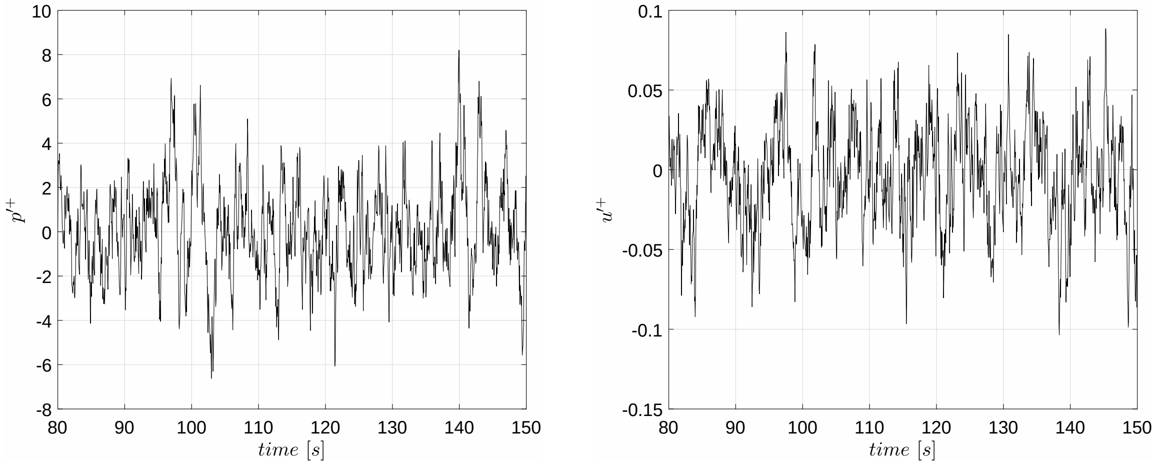

(a) p' at half channel height

(b) u'_x at half channel height

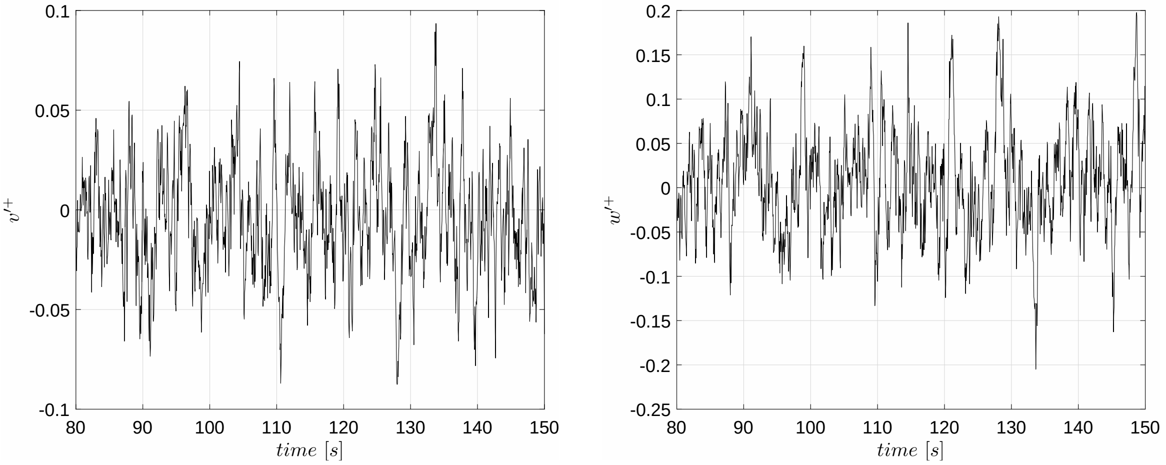

(c) u'_y at half channel height

(d) u'_z at half channel height

Figure 6.9: Pressure and Velocity fluctuations at a single point at the half channel height in time. The '+' symbol indicates that the values of the pressure and velocity fluctuations have been normalized by the wall friction velocity u_τ.

spectrum model does not provide good estimation for smaller eddy length scales (k_{kol}). Therefore, the model needs a better approximation of energy spectrum for wavenumbers $k \approx k_{kol}$ to produce a better correlation with DNS results.

Table 6.8 compares the different characteristics of the flow. For a proper comparison all the data has been normalized with friction velocity, u_τ. It can be observed from the table that near the wall, the RMS of total pressure (p_{RMS}) from the pressure fluctuation model and the standard URANS model are observed to be underestimated in comparison to DNS results. At the centre, the p_{RMS} is overestimated for the pressure fluctuation model and the remains underestimated for the standard URANS model. A reverse trend can be observed in the case of turbulent kinetic energy. At Point A ($y^+ \approx 4$), the values of K are overestimated compared to DNS and the values at Point B it's underestimated. The second observation is that the p_{RMS} at near the wall and at half channel height are nearly the same for the pressure fluctuation model and the standard URANS model. This observation brings in light the diffusive effects of 2-equation RANS models that are based on Boussinesq hypothesis. The deviation in the value of K could also be due to the inaccuracy of near wall calculations where viscous forces tend to dominate. Moreover, since the model assumes isotropy, the transport of eddies due to pressure-strain interactions are neglected. This assumption can underestimate the shear stresses and leads to lower values of pressure fluctuations. The RMS (Root Mean Squared) values of near wall pressure fluctuations p_{RMS} are 50% lower when compared to DNS results. But taking into account the p_{RMS} from the standard URANS model, it can be observed that the pressure fluctuation model is a much better approximation for an FSI simulation. Apart from the RANS models, the results obtained are

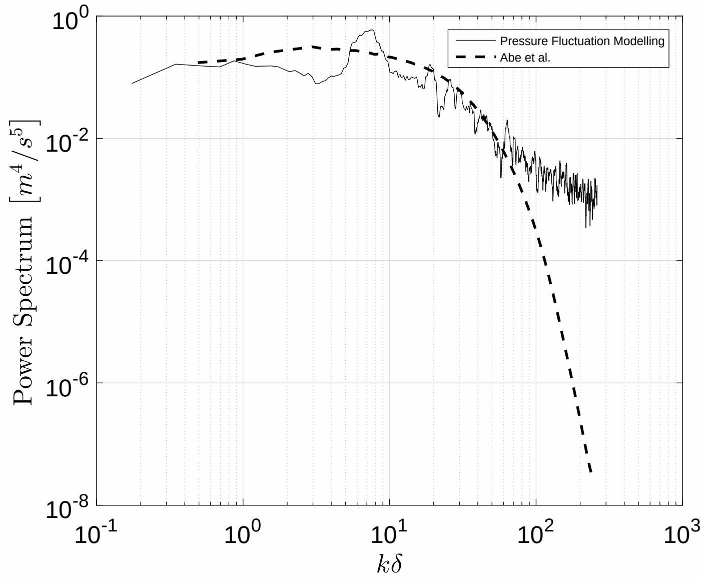

Figure 6.10: The figure depicts the comparison of power spectrum of the turbulent pressure fluctuations of the DNS database [28] and the Pressure Fluctuation Model as a function of $k\delta$ at $y^+ = 10$. Where k is the wavenumber and δ the channel height.

$Re_\tau = 640$			
Case	Position	p_{rms}	TKE
DNS results [28]		2.36	0.0239
Pressure Fluctuation Model	Point A	1.41	0.09
$k-\omega$ model		0.000228	0.09
DNS Results [28]		0.746	0.771
Pressure Fluctuation Model	Point B	1.47	0.622
$k-\omega$ model		0.000221	0.622

Table 6.8: Comparison between the RMS of total pressure p_{RMS} and the Turbulent Kinetic Energy (TKE) of the flow obtained from DNS database, U-RANS model with pressure fluctuation model and the standard URANS model. The total pressure can be defined as $p = \overline{p} + p'$.

also sensitive to factors such as the mesh, discretization schemes, and time steps. It can be hence be concluded that the intensity of pressure fluctuations are dependent on proper values of Turbulent Kinetic energy K to obtain a good correlation between the pressure fluctuation model and DNS results.

In a fluid structure interaction problem, we are more concerned with the near wall pressure fluctuations as the traction forces on the structure are calculated through these pressure fluctuations. It was observed that the modelled turbulent pressure fluctuations are under-estimated near the wall. Due to the lower values of the turbulent pressure field, we can also expect a more conservative result obtained from a coupled simulation, when compared to a high fidelity fluid solver.

6.2.2. Steel flap in turbulent Water flow

The steel flap in a turbulent water case is a variation of the numerical benchmark test case by Turek and Hron [9]. This is a 2-dimensional, numerical test case consisting of a cantilever steel flap with the same orientation as the fluid flow. The fluid flow (water) around the flap is turbulent in nature. This turbulent flow causes pressure fluctuations on the flap, causing vibrations. This case is to test the feasibility of pressure fluctuation modelling for simulating Turbulent Induced Vibrations (TIV). Figure 6.11 gives a clear picture of the mesh and the domain size that was used for the simulating TIV.

Simulation set-up

The simulation was performed by coupling the FVM code OpenFOAM and the FEM code Deal.II. Since the mesh used is non conformal, the mesh interpolation was carried out using the *Thin-plate-spline* radial basis function. The left boundary of the mesh is considered as a velocity inlet, the right boundary

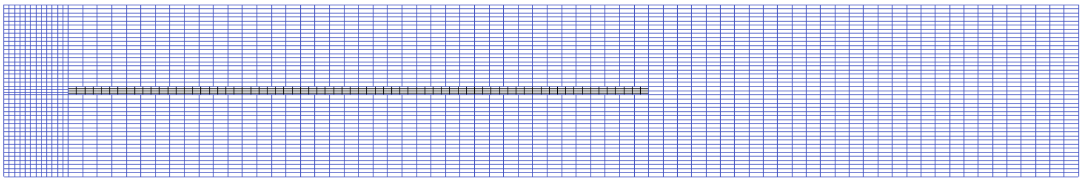

Figure 6.11: Mesh and domain of the Steel Flap in Turbulent Water test case. The length of the fluid domain (in blue) $L = 2.5\ m$, height of the fluid domain $H = 40\ mm$, length of the flap (in black) $l = 1.35\ m$ and the width of the flap $h = 0.2\ mm$. The left end of the steel flap is provided a fixed boundary condition, and the right end of the flap is free resulting in a cantilever beam.

Fluid Properties (Water)	
Density (ρ_f)	$1000\ kg/m^3$
Kinematic Viscosity (ν_f)	$1 \times 10^{-6}\ m^2/s$
Structural Properties (Steel)	
Density (ρ_s)	$7850\ kg/m^3$
Elasticity Modulus	$210\ GPa$
Poisson Ratio	0.33

Table 6.9: Material properties used in flexible steel flap in water experiment.

is the pressure outlet. The top and bottom boundaries of the domain are considered as walls with no-slip condition. The solid on the other hand is a cantilever beam, depicted by the mesh in black color in figure 6.11. The left boundary of the domain is given the Dirichlet boundary condition with zero displacement in all the directions. The other surface patches of the mesh are free to move. Only the patch of the fluid mesh in contact with the solid beam is free to move, with the relative velocity and displacement at the interface being zero. All the other boundaries in the fluid domain are fixed. The mesh of the structure and the fluid are composed of quadrilateral mesh cells, since the simulation is a 2-Dimensional case. A time step of $1\ ms$ was used in the simulation, with a second order temporal scheme.

The coupling algorithm used in this case, was the IQN-ILS (Interface Quasi Newton with Inverse Jacobian estimate by Least Squared Method). The inlet velocity of water is $3\ m/s$ and the bulk Reynolds Number is 1.2×10^6, considering the inlet velocity as the bulk velocity and the channel height as the length scale. The working fluid used here is water and the solid is steel, the properties of the same have been mentioned in table 6.9. Since the Reynolds number is sufficiently high the flow of water is turbulent. Due to high turbulence, the pressure fluctuations provide external excitation on the solid body. The FSI simulation was performed using a standard U-RANS model (standard $k - \omega$). The first case was performed without the use of pressure fluctuation modelling, and the second simulation was performed with the use of pressure fluctuation modelling. The final results are then compared and analysed.

Case	Natural Frequency [Hz]	RMS Amplitude $[\times 10^{-3}\ m]$
Analytical (in vacuum)	91.67	–
Standard $k - \omega$ (in water)	76.9	0.014
Pressure Fluctuation Model (in water)	76.25	0.379

Table 6.10: Comparison of the calculated natural frequencies of the system by FFT (Fast Fourier Transforms) of the beam displacement at the free end with respect to time. The analytical calculations are performed to calculate the natural frequency of a cantilever beam in vacuum. Due to the added-mass effect of the water, the natural frequency of the steel flap is seen to decrease by approximately 16%. The main observation can be made in the comparison of the RMS amplitudes of the beam. The amplitude resulting from pressure fluctuation model are $30\times$ higher compared to the standard $k - \omega$ model.

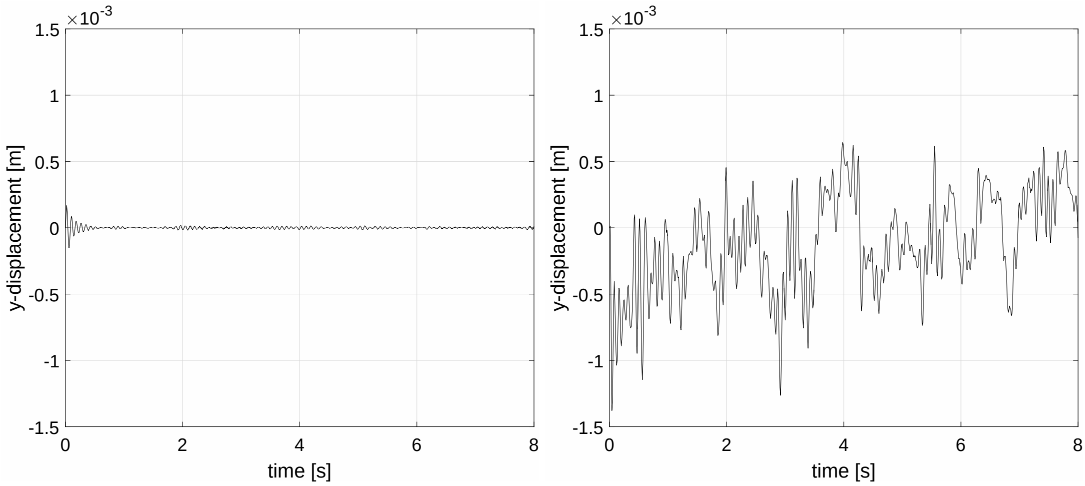

(a) Vertical displacement of the free-end of the beam without pressure fluctuation modelling.

(b) Vertical displacement of the free-end of the beam with pressure fluctuation modelling.

Figure 6.12: Comparison between the displacements of the free end of the beam obtained from the FSI test case, with and without the pressure fluctuation model. The vibrations from the $k-\omega$ are seen to damp out, whereas, the vibrations from the pressure fluctuation model are self-sustained.

Results and Discussions

Figure 6.12 shows the comparison between the vertical displacements of the free-end (refer figure 6.11) of the cantilever beam for both the cases. It can be observed that in the standard case, when the pressure fluctuation model is not used, there is a large initial displacement observed due to the developing flow along the beam. After the flow is fully developed, the beam vibrations are significantly damped out, and displacement amplitudes of in the order of $10^{-5}\ m$ can be observed. This behaviour is also observed in the study by Eline et al. [22]. However, when the pressure fluctuation model is used, it can be observed the vibrations induced on the beam do not damp out, and there is a continuous random excitation due to externally applied pressure fluctuations.

These external excitations on the beam simulate the effect of TIV. The amplitudes of the vibration in this case are 2 orders of magnitude higher than the initial test case performed. The frequency of the vibrations have been analysed and is tabulated in table 6.10. It can be observed that both the methods predict a similar natural frequency of the beam which is also in accordance with the studies performed by Eline et al. [22] and De Ridder [20]. With the pressure fluctuation model, it is observed that the amplitude of the vibrations is an order of magnitude higher compared to a standard U-RANS model.

By use of a standard U-RANS models in FSI simulations one cannot predict the amplitudes of structural vibrations due to excessive damping. However, with the use of pressure fluctuation modelling it is possible to estimate the amplitudes of vibrations of the structures. Furthermore, it is also possible to estimate the critical velocity of the system which leads to fluid-elastic instability.

Although the model succeeds at generating the required behaviour of the structure, it is yet to be validated with experimental cases. Further focus would be given to validating this method to solve application based problems in the future.

7

Conclusions

In this thesis work, an elaborate study was made on the causes of FIV (Flow Induced Vibrations) and TIV (Turbulence Induced Vibrations) on slender structures in nuclear reactor applications. The closely packed slender rods are subjected to pressure fluctuations due to turbulent flow of coolants around them, which can develop into periodic pressure pulsations, leading to fluid elastic instabilities. The initiation of FIV is usually due to externally induced excitation. The most common source of these excitation are turbulent pressure fluctuations. The current study was focused on the ways to simulate TIV for axial flow conditions. Literature study showed that the state of the art methods of simulating Turbulence induced vibrations use high fidelity fluid solvers such as DNS or LES [3]. But the usage of high fidelity is an expensive method which is not feasible for industrial use. The task of reducing the computational expenses brought forth the main question during the course of the thesis, ***Is it possible to simulate Turbulence Induced Vibrations using low fidelity solvers using RANS models?***

Focusing on the research question, studies were then based on the use of URANS for simulating TIV by partitioned coupling of fluid and structure solvers. Two methods for this were explored within the thesis, the first method is to externally induced vibrations through an initial perturbation consisting of an impulse or a uniform body force. The second method is to model pressure fluctuations from the turbulent quantities calculated in the U-RANS solver and mapping the fluctuating pressure field onto the structure solver, triggering the vibrations.

For simulating TIV through initial perturbations, three experimental cases were simulated and compared to experimental results.

- *Test case-I*: The Vattenfall-I case, was a simple laminar case, which validated the use of use of the Gauss-Seidel coupling scheme and the use of FEM-FVM coupling. No stability issues were observed with use of Gauss-Seidel coupling scheme. It was also concluded that FEM discretization is more efficient for solid solvers and can lead to a faster convergence compared to an FVM-FVM coupling.

- *Test case-II*: In the Vattenfall-II experimental case, the simulation of turbulence vibrations was performed using two different URANS model. Since, the use of the FVM-FEM combination resulted in a computationally cheaper solution; it was preferred over using the FVM-FVM combination. The URANS models used for the test case were the $k - \omega\ SST$ and the RSM (Reynolds Shear-stress Model). From the results we conclude that the natural frequencies, mainly the first modes of the structures, can be predicted accurately.

- *Test case-III*: The simulation of the Flexible brass beam in turbulent water case was performed to validate the effects of the varying inlet velocities on the natural frequency of the structure. Three inlet velocities $10\ m/s$, $20\ m/s$, and $30\ m/s$ were selected to validate the test case. Although a deviation of 10% was observed in the values of natural frequencies, the trend of the natural frequency dependence on the flow velocities were similar. The natural frequencies are observed to be a linear function of the flow velocity with a negative slope. Whereas, the damping ratios was found to be an increasing linear function of the inlet velocity. Hence, it can be concluded that the behaviour of the beam is accurately predicted in comparison to the experiments through the use of URANS models.

An important conclusion from Test cases II and III, is that the URANS models do not have direct influence on an FSI simulation for simulating TIV. In FSI simulations with standard URANS models, the traction on the structure is calculated with the use of the time or ensemble averaged quantities. Therefore, only the time or ensemble averaged effect of turbulent fluctuations on the flow are taken into account. However, for simulating structural vibrations a detailed variation of the turbulent fluctuations over time is needed. Hence, the URANS models can only predict the natural frequencies and modal damping ratios accurately. However, The turbulence models are incapable of simulating external excitation on the structure solver. This results in the damping out of the vibrations that are initiated through the external perturbation.

In chapter 4, the second method is explored which involved modeling of turbulent pressure fluctuations. These pressure fluctuations act as an external excitation causing the solid beam to vibrate. The model focuses on the usage of isotropic turbulence assumption. To validate the method, an initial simulation of a turbulent plane channel flow was performed with $Re_\tau = 640$ and compared to DNS results by Abe et al. [28]. The RMS value of pressure fluctuations modelled near the wall are under-estimated when comparable to the DNS results. These modelled pressure fluctuations in an FSI simulation will lead to lower amplitudes of vibrations compared to high fidelity solvers while simulating TIV.

After validating the model with a fluid only test case, the FSI simulation of TIV was performed as the next step. For this a 2-dimensional numerical test case was chosen. The test case was of a cantilever steel flap in turbulent water flow, with the flow being along the longitudinal axis of the beam. This test case was performed using a U-RANS model, with and without the use of pressure fluctuation model. The results of these two cases were then compared to check the feasibility of the results. It was observed from the results that the standard U-RANS model without pressure fluctuation model damps the vibrations of the beam, whereas, the in the other case, the modelled pressure fluctuations continue to generate vibrations of the beam, and the beam is seen to vibrate in a random fashion, as expected in a turbulent flow.

The above discussions shows the possibility of the usage of U-RANS models with the usage of a pressure fluctuation model to simulate TIV. The initial results obtained from section 6.2.2 show that the inclusion of a pressure fluctuation modeling within the fluid solver can simulate the behaviour of solid similar to that observed in TIV.

7.1. Recommendations

This pressure fluctuation method should be further validated with experimental test cases to check the accuracy of this method and to refine the solver further. Models with for energy spectrum estimation with anisotropic turbulence should also be looked into. The anisotropic model can then be used in conjunction with Reynolds Shear stress turbulence model (RSM), which can then be validated with the experiments and DNS results.

A

pimpleFluct Solver - Main Code

```
/*---------------------------------------------------------------------------*\
Application
    pimpleFluct

Description
    Large time-step transient solver for incompressible, flow using the PIMPLE
    (merged PISO-SIMPLE) algorithm.

    Turbulence modelling is generic, i.e. laminar, RAS or LES may be selected.

    Modelling pressure and velocity fluctuations using RANS models.
\*---------------------------------------------------------------------------*/

#include "fvCFD.H"
#include "Random.H"
#include "vector.H"
#include "vectorList.H"
#include "createFunctions.H"
#include "singlePhaseTransportModel.H"
#include "turbulenceModel.H"

// * * * * * * * * * * * * * * * * * * * * * * * * * * * * * * * * * * * * * //

int main(int argc, char *argv[])
{
#   include "setRootCase.H"
#   include "createTime.H"
#   include "createMesh.H"
#   include "createFields.H"
#   include "createMoreFields.H"
#   include "randomValueGenerator.H"
#   include "initContinuityErrs.H"

// * * * * * * * * * * * * * * * * * * * * * * * * * * * * * * * * * * * * * //

    Info<< "\nStarting␣time␣loop\n" << endl;

    while (runTime.run())
```

```
    {
#       include "readTimeControls.H"
#       include "readPIMPLEControls.H"
#       include "CourantNo.H"
#       include "setDeltaT.H"

        runTime++;

        Info<< "Time␣=␣" << runTime.timeName() << nl << endl;

        // --- Pressure-velocity PIMPLE corrector loop
        for (int oCorr = 0; oCorr < nOuterCorr; oCorr++)
        {
            if (nOuterCorr != 1)
            {
                p.storePrevIter();
            }

#           include "UEqn.H"

            // --- PISO loop
            for (int corr = 0; corr < nCorr; corr++)
            {
#               include "pEqn.H"
            }

            turbulence->correct();
        }

        runTime.write();

        // --- Pressure Fluctuation Modelling Calculations
        if (runTime.value() >= stabTime)
        {
#           include "velocityFluct.H"
        }
        else
        {
            pTurb.internalField() = 0;
            pTurb.boundaryField() = 0;
        }
        Info<< "ExecutionTime␣=␣" << runTime.elapsedCpuTime() << "␣s"
            << "␣␣ClockTime␣=␣" << runTime.elapsedClockTime() << "␣s"
            << nl << endl;
    }

    Info<< "End\n" << endl;

    return 0;
}


// ************************************************************************* //
```

B

Libraries

B.1. velocityFluct.H

```
scalar tCurrent = runTime.value();
scalar dtValue = runTime.deltaTValue();
scalar tOld = runTime.startTime().value();

//---------- Extract Fields from the turbulence model -------------------------


tmp<volScalarField> eps = turbulence->epsilon();

nTimes = ((tCurrent - tOld)/dtValue)+1;// number of sub-timeSteps

modesList = linSpace(1,nModes,nModes);

tmp<volScalarField> ke = turbulence -> k();

tmp<volScalarField> omega_ = eps()/ke();


//-------- Compute the large eddy and kolmogorov wave numbers --------------

kappaKol = 2*pi*Foam::pow(eps()/Foam::pow(nu, 3),0.25);

lEddy = Foam::pow(ke(),1.5)/eps();

kappaEddy = 2*pi/lEddy;

tKol = Foam::sqrt(nu/eps());

//---------- Iterations for beta --------------------------------------------

#include "betaIter.H"

//---------- cell-wise loop for calculating velocity fluctuations ----------

Info << "Entering␣cellwise␣loop" << endl;
```

```
forAll(mesh.C(),cellI)
{
    #include ”cellCalc.H”
}
Info << ”uFluct␣::” << uFluct.average() << endl;

//————————— Solve for pressure Fluctuations ——————————————————————

#include ”solveTurbPress.H”

Info << ”Pressure␣Fluctuation␣Average::␣”<< pTurb.average() << endl;
```

B.2. betaIter.H

```
dimensionedScalar tCurrent_
(
    ”tCurrent_”,
    dimensionSet(0,0,1,0,0,0,0),
    tCurrent
);
dimensionedScalar tOld_
(
    ”tOld_”,
    dimensionSet(0,0,1,0,0,0,0),
    tOld
);

kappaE = Foam::pow(ke(),−1.5)
         * eps()
         * Foam::pow(1.5,1.5)
         * Foam::pow(2,(−17/4));
Info <<”Avg kappE ”<< kappaE.average() << endl;
beta = 2 * nu * Foam::pow(kappaE,2);
Info << ”Beta Value::” << beta.average() << endl;
A = 3 / 7.12719 / intfVol(beta,dEta,tKol,dimlessVar);
Info << ”A :: ” << A.average() << endl;
```

B.3. cellCalc.H

```
//position vector
vector posVec = centres[cellI];

//dKappa
dKappa = (Foam::log(kappaKol[cellI])
          −Foam::log(kappaEddy[cellI]))/(nModes−1);

if(dKappa >0){
    //kappa (1,nModes)
    kappa = Foam::exp((modesList−1)*dKappa)*kappaEddy[cellI];

    //kappa (1,nModes)
    if (kappaE[cellI] <= kappaEddy[cellI])
    {
        dKappa = (Foam::log(kappaKol[cellI])
                  − Foam::log(kappaE[cellI]))
```

```
                  / (nModes-1);
        kappa = Foam::exp((modesList-1)*dKappa)*kappaE[cellI];
    }


    scalar C = 1;
    scalar D = 1;
    for (int i = 0 ; i < nModes; i++ )
    {
        C = kappa[i]/kappaE[cellI];
        D = 1 + C*C;
        scalar k_ = -2*nu.value()*tKol[cellI]*Foam::pow(kappa[i],2);
        eKappa[i] = A[cellI] * 2 * ke()[cellI] * 7.12719 / 3 / kappaE[cellI]
                    * Foam::pow(C,4) / Foam::pow(D,2.8334) *  Foam::exp(k_);
        X[i] = randX[cellI][i];
    }

    theta = Foam::acos(1-(2*X));
    alpha = Foam::atan(-1/Foam::cos(theta));
    psi = 2*pi*X; // previously labelled phi
    phase = pi*X;
    vectorList UcVec = vectorList(nModes);

    for (int i = 0 ; i < nModes; i++ )
    {

        kappaVec[i] = vector(
          kappa[i] * Foam::sin(theta[i]) * Foam::cos(psi[i]),
          kappa[i] * Foam::sin(theta[i]) * Foam::sin(psi[i]),
          kappa[i] * Foam::cos(theta[i])
        );

        omega[i] = Foam::pow(eps()[cellI],(1/3)) * Foam::pow(kappa[i],(2/3));

        sigma[i] = vector(
          (Foam::cos(alpha[i])) * Foam::cos(psi[i])
            - Foam::cos(theta[i]) * Foam::sin(psi[i]) * Foam::sin(alpha[i]),
          (Foam::cos(alpha[i])) * Foam::sin(psi[i])
            + Foam::cos(theta[i]) * Foam::cos(psi[i]) * Foam::sin(alpha[i]),
          (Foam::sin(alpha[i]) * Foam::sin(theta[i]))
        );

       UcVec[i] = 0.57735* vector (
            omega[i]/kappaE[cellI],
            omega[i]/kappaE[cellI],
            omega[i]/kappaE[cellI]
       );
    }

//  Info << ”sigma” << sigma << endl;

    Uc =  omega/kappaE[cellI]; //convection velocity
    scalarList zeta = scalarList(nModes);
    scalar maxKRatio =0;

//  Info << ”sigma ” << sigma << endl;
```

```
        for  (int j = 0; j < nModes; j++ )
        {
            zeta[j] = (posVec - UcVec[j]*(tCurrent-tOld)) & kappaVec[j];
            uAmp[j] = kappa[0]
                      * Foam::exp(scalar(j) * dKappa)
                      * (Foam::exp(dKappa) - 1)
                      * eKappa[j]
                      / absolute( Foam::cos( zeta[j]
                                             + phase[j]
                                             + (tCurrent-tOld)
                                             *omega[j]
                                            )
                                 )
                      * 0.8165
                      * Foam::sqrt(1/ke()[cellI]);
        }

        // Starting to calculate the ampiltude for the fluctuating signal
        ufluct = vector::zero;

        for (int i = 0; i < 3; i++)
        {
            for (int k = 0; k < nModes; k++)
            {
                    zeta[k] = (posVec - (tCurrent-tOld)
                              * UcVec[k]) & kappaVec[k];
                ufluct[i] = ufluct[i]
                              +  uAmp[k]
                              * sigma[k][i]
                              * Foam::cos( zeta[k]
                                           + phase[k]
                                           + (tCurrent-tOld)
                                           *omega[k]
                                          );
            }
            uFluct[cellI][i] = ufluct[i];
        }
    }
    else{
        uFluct[cellI].replace(0,0.8165*Foam::sqrt(ke()[cellI]));
        uFluct[cellI].replace(1,0.8165*Foam::sqrt(ke()[cellI]));
        uFluct[cellI].replace(2,0.8165*Foam::sqrt(ke()[cellI]));
    }
```

B.4. solveTurbPress.H

```
    uFluctSqr.component(symmTensor::XX) = uFluct.component(vector::X)
                                             * uFluct.component(vector::X);
    uFluctSqr.component(symmTensor::XY) = uFluct.component(vector::X)
                                             * uFluct.component(vector::Y);
    uFluctSqr.component(symmTensor::XZ) = uFluct.component(vector::X)
                                             * uFluct.component(vector::Z);
    uFluctSqr.component(symmTensor::YY) = uFluct.component(vector::Y)
                                             * uFluct.component(vector::Y);
```

```
uFluctSqr.component(symmTensor::YZ) = uFluct.component(vector::Y)
                                        * uFluct.component(vector::Z);
uFluctSqr.component(symmTensor::ZZ) = uFluct.component(vector::Z)
                                        * uFluct.component(vector::Z);

phiTurb = (fvc::interpolate(uFluct) & mesh.Sf());
scalar pIter = 0;
convectivePhi = fvc::interpolate(myForce) & mesh.Sf();
adjustPhi(phiTurb, uFluct, pTurb);

while(pIter < 1)
{
    fvScalarMatrix pTurbEqn
    (
    fvm::laplacian(pTurb) == -2*fvc::div(fvc::div(phiTurb,U))
                             - fvc::div(fvc::div(uFluctSqr))
                             + fvc::div(convectivePhi)
    );
    pTurbEqn.setReference(pRefCell,pRefValue);
    pTurbEqn.solve();
    pIter += 1;
}
```

Bibliography

[1] JSME, *Flow Induced Vibrations*, edited by S. Kaneko, T. Nakamura, F. Inada, M. Kato, and N. W. Mureithi (Elsevier, 2008).

[2] J. Degroote, *Archives of computational methods in engineering,* (Springer International Publishing, 2013) Chap. Partitioned Simulation of Fluid-Structure Interaction, Coupling Black-Box Solvers with Quasi-Newtion Techniques.

[3] Z. G. Liu, Y. Liu, and J. Lu, *Numerical simulation fluid-structure interaction for two simple fuel assemblies,* Nuclear Engineering and Design (2013).

[4] W. Thompson, *Vibration Theory and Applications* (Prentice-Hall, Englewood Cliffs, 1965).

[5] A. H. Zuijlen, *Simulation of fluid-structure interaction, coupling in time with higher order accuracy,* Lecture Notes.

[6] C. Broyden, *A class of methods for solving nonlinear simultaneous equations,* Mathematics for Comuputation **19** (1965).

[7] J. Degroote and J. Vierendeels, *Multi-level quasi-newton coupling algorithms for the partitioned simulation of fluid-structure interaction,* Computtational Methods Applications in Mechanical Engineering (2012).

[8] D. S. Blom, A. H. Zuijlen, and H. Bijl, *Acceleration of strongly coupled fluid- sturcture interaction with manifold mapping,* (2015).

[9] S. Turek and J. Hron, *Proposal for numerical benchmarking of fluid-structure interaction between an elastic object and laminar incompressible flow.* (2006).

[10] A. E. J. Bogaers, S. Kok, B. D. Reddy, and T. Fanz, *Quasi-newton methods for implicit black-box fsi coupling,* Computational Methods Application in Mechanical Engineering (2014).

[11] M. V. Dyke, *An Album of Fluid Motion* (The Parabolic Press, 1982).

[12] L. F. Richardson, *Weather prediction by numerical process* (Cambridge Univeristy Press, 1922).

[13] W. P. Breugem, *Turbulence a course - lecture notes,* .

[14] J. Smagorinsky, *General Circulation Experiments with the Primitive Equations*, Vol. 91 (Monthly Weather Review, 1963).

[15] H. Tennekes and J. L. Lumley, *A First Course in Turbulence* (The MIT Press, 1972).

[16] W. P. Jones and B. E. Launder, *The prediction of laminarization with a two-equation model of turbulence,* International Journal of Heat and Mass Transfer **15** (1972).

[17] D. C. Wilcox, *Re-assessment of the scale-determining equation for advanced turbulence models,* AIAA Journal (1988).

[18] B. Launder, G. J. Reece, and W. Rodi, *Progress in the development of a reynolds-stress turbulent closure,* Journal of Fluid Mechanics **68(3)** (1975).

[19] CFD-Online, *Reynolds stress model (rsm),* `www.cfd-online.com/Wiki/Reynolds_stress_model_(RSM),` .

[20] J. D. Ridder, J. Degroote, K. Tichelen, and P. Schuurmans, *Modal characteristics of a flexible cylinder in turbulent axial flow from numerical simulations,* Journal of Fluids and Structures (2013).

[21] S. S. Chen and M. W. Wambsganns, *Parallel flow induced vibration of fuel rods,* Nuclear Engineering and Design (1972).

[22] E. ter Hofstede, S. Kottapalli, and A. Shams, *Numerical prediction of flow induced vibrations for safety in nuclear reactor applications,* in *CFD4NRS-6* (Massachusetts Institute of Technology, MA, 2016).

[23] S. Senthooran, *A Computational Model to Calculate Flow-Induced Pressure Fluctuations on a Bluff Body*, Ph.D. thesis, Texas Tech University (2002).

[24] J. O. Hinze, *Turbulence* (Mc-Graw Hill, 1975).

[25] D. Thompson, E. Iglesias, X. Liu, J. Zhu, and Z. Hu, *Recent developments in the prediction and control of aerodynamic noise from high-speed trains,* International Journal of Rail Transportation (2015).

[26] D. Juve', M. Berton, and E. Salze, *Flow induced noise and vibration issues and aspects,* (Springer International Publishing, 2015) Chap. Spectral Properties of Wall-Pressure Fluctuations and Their Estimation from Computational Fluid Dynamics.

[27] W. Bangerth, D. Davydov, T. Heister, L. Heltai, G. Kanschat, M. Kronbichler, M. Maier, B. Turcksin, and D. Wells, *The `deal.II` library, version 8.4,* Journal of Numerical Mathematics **24** (2016).

[28] H. Abe, H. Kawamura, and Y. Matsuo, *Direct numerical simulation of a fully developed turbulent channel flow with respect to the reynolds number dependence,* American Society of Mechanical Engineers (2001).

[29] E. Lillberg, K. Angele, G. Lundqvist, and N. Edh, *Tailored experiments for validation of cfd with fsi for nuclear reactor applications,* in *NURETH16* (Chicago, IL, 2015).

[30] E. Lillberg, *Energiforsk FIV Experiment, Data for Computational Analysis*, Tech. Rep. (Vattenfall, Stockholm, Sweden, 2015).

[31] Vu and T. Truc, *Testing and optimization of unicorn fluid-structure Interaction solver for simuting an industrial problem*, Master's thesis, KTH Computer Science and Communication (2014).